

LOW AND HIGH IONIZATION ABSORPTION PROPERTIES OF Mg II ABSORPTION-SELECTED GALAXIES AT INTERMEDIATE REDSHIFTS. II. TAXONOMY, KINEMATICS, AND GALAXIES^{1,2}

CHRISTOPHER W. CHURCHILL³, RICHARD R. MELLON, JANE C. CHARLTON⁴

The Pennsylvania State University, University Park, PA 16802

BUELL T. JANNUZI

National Optical Astronomy Observatories, Tucson, AZ 85719

SOFIA KIRHAKOS

Institute for Advanced Study, Princeton, NJ 08544

CHARLES C. STEIDEL⁵

California Institute of Technology, Palomar Observatories, Pasadena, CA 91125

AND

DONALD P. SCHNEIDER

The Pennsylvania State University, University Park, PA 16802

The Astrophysical Journal, submitted

ABSTRACT

We examine a sample of 45 Mg II absorption-selected systems over the redshift range 0.4 to 1.4 in order to better understand the range of physical conditions present in the interstellar and halo gas associated with intermediate redshift galaxies. Mg II and Fe II absorption profiles were observed at a resolution of $\simeq 6 \text{ km s}^{-1}$ with HIRES/Keck. Ly α and CIV data were measured in FOS spectra obtained from the *Hubble Space Telescope* archive (resolution $\simeq 230 \text{ km s}^{-1}$). We perform a multivariate analysis of $W_r(\text{Mg II})$, $W_r(\text{Fe II})$, $W_r(\text{CIV})$ and $W_r(\text{Ly}\alpha)$ (rest-frame equivalent widths) and the Mg II kinematic spread. There is a large range of high-to-low ionization properties and kinematics in intermediate redshift absorbers, that we find can be organized into five categories: “Classic”, “CIV-deficient”, “Single/Weak”, “Double”, and “DLA/Hi-Rich”. These categories arise, in part, because there is a strong connection between low-ionization kinematics and the location of an absorber on the $W_r(\text{CIV})$ – $W_r(\text{Mg II})$ plane. Using photoionization modeling, we infer that in most absorbers a significant fraction of the CIV arises in a phase separate from that giving rise to the Mg II. We show that many of the CIV profiles are resolved in the FOS spectra due to velocity structure in the CIV gas. For 16 systems, the galaxy M_K , M_B , $B - K$, and impact parameters are measured. We compare the available absorption-line properties (taken from Churchill et al. 1999, Paper I) to the galaxy properties but find no significant (greater than 3σ) correlations, although several suggestive trends are apparent. We compare the locations of our intermediate redshift absorbers on the $W_r(\text{CIV})$ – $W_r(\text{Mg II})$ plane with those of lower and higher redshift data taken from the literature and find evidence for evolution that is connected with the Mg II kinematics seen in HIRES/Keck profiles of Mg II at $z > 1.4$. We discuss the potential of using the above categorizations of absorbers to understand the evolution in the underlying physical processes giving rise to the gas and governing its ionization phases and kinematics. We also discuss how the observed absorbing gas evolution has interesting parallels with scenarios of galaxy evolution in which mergers and the accretion of “proto-galactic clumps” govern the gas physics and provide reservoirs for elevated star formation rates at high redshift. At intermediate and lower redshifts, the galaxy gaseous components and star formation rates may become interdependent and self-regulatory such that, at $z \leq 1$, the kinematics and balance of high and low ionization gas may be related to the presence of star forming regions in the host galaxy.

Subject headings: quasars— absorption lines; galaxies— evolution; galaxies— halos

1. INTRODUCTION

It is well known that individual galaxies fall into a fairly clear-cut morphological classification scheme, as first proposed by Hubble (1936). Over the decades, Hubble’s scheme has been expanded upon and exploited for quantifying galactic evolution, galactic stellar populations and star formation efficiencies, the

relative gas-phase component to stellar component in galaxies, and the effects of environment on galaxy formation. Similarly, one of the central motivations for studying intervening quasar absorption lines, especially those selected by the presence of metal lines, is that they also provide insights into galactic evolution, not of the stars and stellar dynamics, but of the chemical, ionization, and kinematic conditions of interstellar and halo

¹Based in part on observations obtained at the W. M. Keck Observatory, which is operated as a scientific partnership among Caltech, the University of California, and NASA. The Observatory was made possible by the generous financial support of the W. M. Keck Foundation.

²Based in part on observations obtained with the NASA/ESA *Hubble Space Telescope*, which is operated by the STScI for the Association of Universities for Research in Astronomy, Inc., under NASA contract NAS5–26555.

³Visiting Astronomer at the W. M. Keck Observatory

⁴Center for Gravitational Physics and Geometry

⁵NSF Young Investigator

gas.

Historically, absorption line systems have been classified in a taxonomic system by their gas cross sections. Categorized by increasing HI column densities are the Ly α forest clouds, with $N(\text{HI}) \leq 10^{15} \text{ cm}^{-2}$, the sub-Lyman limit systems, having $N(\text{HI}) \sim 10^{16} \text{ cm}^{-2}$, the Lyman limit break systems, with $N(\text{HI}) \geq 10^{17.3} \text{ cm}^{-2}$, and the damped Ly α systems, having $N(\text{HI}) \geq 10^{20.3} \text{ cm}^{-2}$. Metal-line systems are either selected by the presence of strong Mg II $\lambda\lambda 2796, 2803$ absorption or strong C IV $\lambda\lambda 1548, 1550$ absorption.

What has not been explored, however, is the taxonomy of absorption line systems when the HI, Mg II, and C IV absorption strengths and the gas kinematics are equally considered. Ultimately, categorizing the relationships between several different absorption properties may provide clues central to understanding the different physical natures of the various types of systems.

Furthermore, while our empirical knowledge of the absorption strengths, kinematics, and physical extent of galaxies selected by Mg II absorption has steadily progressed over the last decade (e.g. Bergeron & Boissé 1991; Lanzetta & Bowen 1990, 1992; Bergeron et al. 1992; Le Brun et al. 1993; Steidel et al. 1994; Churchill et al. 1996; Guillemin & Bergeron 1997), little is *directly* known about HI absorption and higher ionization absorption (esp. Si IV, C IV, N V, and O VI) in these galaxies.

Arguably, the Mg II-selected systems are ideally suited for a taxonomic study of absorption systems because:

(1) those with $W_r(\text{Mg II}) \geq 0.3 \text{ \AA}$ are known to be directly associated with galaxies (Bergeron & Boissé 1991; Steidel, Dickinson, & Persson 1994; Churchill et al. 1996) and/or sub-galactic metal-enriched environments (Yanny 1992; Yanny & York 1992). *HST* imaging has revealed that these galaxies have a wide variety of line-of-sight orientations and “normal” morphologies (see Steidel et al. 1997; Steidel 1998). Since magnesium is an α -group element yielded by Type II supernovae, it is expected that the association with galaxies will hold to the highest redshifts.

(2) they arise in structures having a five decade range of HI column densities, including sub-Lyman limit systems (Churchill et al. 1999a; Churchill et al. 2000, hereafter Paper I), Lyman limit systems (e.g. Steidel & Sargent 1992; Paper I), and damped Ly α systems (e.g. Le Brun et al. 1997; Rao & Turnshek 1998; Boissé et al. 1998) which means that a large range of galactic environments will be sampled.

(3) for $z < 2.2$ their statistical properties and for $z < 1.4$ their kinematic properties have been thoroughly documented (e.g. Lanzetta, Turnshek, & Wolfe 1987; Sargent, Boksenberg, & Steidel 1988; Steidel & Sargent 1992; Petitjean & Bergeron 1990; Steidel & Sargent 1992; Churchill 1997; Churchill et al. 1999a) which means that the low redshift database is already in place and can be used for evolution studies when higher redshift data are obtained.

(4) they are seen to give rise to a range of C IV and other high ionization absorption in UV space-based spectra (Bergeron et al. 1994; Paper I), which means that the more general ionization conditions can be studied in detail (e.g. Churchill & Charlton 1999).

In this paper, we study the combined available data on a sample of 45 Mg II absorption-selected systems at redshifts ~ 0.4 – 1.4 . We focus on the Mg II and Fe II absorption strengths and kinematics, the Ly α and C IV absorption strengths (Paper I), and the ground-based derived galaxy luminosities, colors, and impact parameters. We perform a multivariate analysis (Babu

& Feigelson 1996; Johnson & Wichern 1992) on the absorption line data in order to objectively quantify systematic differences between and/or groupings of the high ionization and neutral hydrogen absorption properties of Mg II selected systems.

The paper is organized as follows: In § 2, we describe the data, the sample selection, and the data analysis. In § 3, we investigate the variation in the high and low ionization properties of intermediate redshift Mg II absorbers using multivariate analysis. We introduce a taxonomy that serves as an objective guide for classifying the variations in Mg II absorber properties. In § 4, we investigate the overall ionization and kinematic conditions. In § 5 we investigate the relationship between the absorption properties and host galaxy properties and in § 6 offer a speculative discussion on the relationships between the absorber classes and their possible evolution. In § 7 we summarize the main points of this work.

2. THE DATA: SAMPLE SELECTION AND ANALYSIS

We targeted quasar absorption line systems at intermediate redshifts that have been discovered by the presence of a Mg II $\lambda\lambda 2796, 2803$ doublet (e.g. Lanzetta, Turnshek, & Wolfe 1987; Sargent, Boksenberg, & Steidel 1988; Steidel & Sargent 1992). We also include in our study the “weak” systems [those with $W_r(\text{Mg II}) < 0.3 \text{ \AA}$], which are more numerous in their redshift path density (Churchill et al. 1999a). A detailed account of the sample selection is given in Paper I, but we briefly outline the sample properties here.

The Mg II absorbers were selected from a high resolution ($\sim 6 \text{ km s}^{-1}$) survey (Churchill 1997) using the HIRES spectrograph (Vogt et al. 1994) on the Keck I telescope. For 45 of these systems, additional wavelength coverage in the ultraviolet was available in the *HST*/FOS archive and the database compiled by the *HST* QSO Absorption Line Key Project (Bahcall et al. 1993; Bahcall et al. 1996; Jannuzi et al. 1998).

The resulting database of Mg II absorbing systems and their rest-frame equivalent widths are listed in Table 1. The first three columns are the quasar name, the absorber redshift, and the Mg II $\lambda 2796$ rest-frame equivalent width, $W_r(\text{Mg II})$. The fourth and fifth columns list the Mg II kinematic spread, ω_v (see Equation 1), and the kinematic composition, i.e. the number of Voigt Profile components (see § 2.2). Columns six, seven, and eight list the Fe II, C IV, and Ly α rest-frame equivalent widths. Column nine gives the various subsamples used for our analyses. Column ten lists the taxonomic “class” of each system (explained in § 3.2).

Full details of the data analysis are given in Paper I, including the continuum fitting, the line finding, the equivalent width measurements, the establishment of a redshift zero point for the FOS spectra, the procedure for line identifications, and the techniques employed to measure Lyman limit breaks, when present.

As shown in Figure 2 of Paper I, the Mg II equivalent width distribution is consistent with that of an unbiased sample of absorbers for $W_r(\text{Mg II}) \leq 1.3 \text{ \AA}$ (Churchill et al. 1999a). There are five systems with $W_r(\text{Mg II}) > 1.3 \text{ \AA}$, which may appear as a bias toward strong systems. When this may be a concern for our analysis, we discuss this possibility.

With regard to detection sensitivity, the sample is 72% complete to a $W_r(\text{Mg II})$ rest-frame detection threshold of 0.02 \AA and 93% complete to a 0.03 \AA threshold (Figure 3 of Paper I). In column nine of Table 1, we have designated those systems having rest-frame detection thresholds greater than 0.03 \AA as Sample A. For these absorbers, unresolved Mg II absorption features

with $W_r(\text{Mg II}) \leq 0.03 \text{ \AA}$ cannot be detected. The other subsample designations, “CA” and IC”, are explained in §§ 3 and 4, respectively.

2.1. Galaxy Sample

For roughly 60 Mg II absorbers having $W_r(\text{Mg II}) \geq 0.3 \text{ \AA}$, Steidel et al. (1994) identified associated galaxies. Only 16 of the 45 Mg II systems presented here, of which 21 have $W_r(\text{Mg II}) \geq 0.3 \text{ \AA}$, have confirmed galaxy counterparts (not all fields studied here have been imaged).

The galaxy properties were obtained from broad-band $g(4900/700)$, $R(6930/1500)$, $i(8000/1450)$ and K -band images of the QSO fields and their redshifts were spectroscopically verified to be coincident (within $\sim 100 \text{ km s}^{-1}$) with those of the Mg II absorbers. PSF subtraction of the quasar was performed for all fields, enabling small impact parameter galaxies to be identified. Further details of the imaging and spectroscopic observations are described in Steidel et al. (1994).

The galaxy properties are presented in Table 2; the columns from left to right are the quasar field, the galaxy redshift, the absolute B magnitude, M_B , the absolute K magnitude, M_K , the de-reddened $B - K$ color, the galaxy-quasar impact parameter in $h^{-1} \text{ kpc}$ ($H_0 = 100 \text{ km s}^{-1} \text{ Mpc}^{-1}$, $q_0 = 0.05$), and a reference if previously published. In a few cases, morphology information is available from published *HST* images (Le Brun et al. 1997; Steidel et al. 1997; Steidel 1998).

It is always possible that a galaxy is misidentified, that another galaxy or more than one galaxy is giving rise to the absorption. Possible selection effects due to misidentifications and incompleteness of galaxy redshifts in the individual quasar fields are discussed by Steidel et al. (1994) and examined in detail by Charlton & Churchill (1996).

2.2. Data Analysis: Kinematics

To measure the kinematic “spread” of the low ionization gas directly from the flux values, we use the second velocity moment of optical depth across the Mg II $\lambda 2796$ profile, defined as,

$$\omega_v = \left\{ \frac{\sum \tau_a(v_i) v_i^2 \Delta v_i}{\sum \tau_a(v_i) \Delta v_i} \right\}^{1/2}, \quad (1)$$

where $\tau_a(v_i) = \ln[I_c(v_i)/I(v_i)]$ is the apparent optical depth measured directly from the flux values (Savage & Sembach 1991) at velocity v_i , $\Delta v_i = (v_{i-1} - v_{i+1})/2$, $v_i = c(\lambda_i/\lambda_{obs} - 1)$, and $\lambda_{obs} = 2796.352(1 + z_{abs})$. The sums are performed only over velocity intervals in which absorption features have been detected at the 5σ level, thus eliminating terms consistent with noise (see Paper I for details on feature detection). The quantity measured by ω_v is similar to the standard deviation measured from a normal distribution. The uncertainty in ω_v is obtained from simple error propagation (Churchill 1997; also see Sembach & Savage 1992). The velocity zero point of each system is set at the median wavelength of the apparent optical depth distribution of the Mg II $\lambda 2796$ profile.

The value of ω_v depends upon the velocity squared, and thus its value is sensitive to the presence of very weak Mg II absorption at large velocity. Therefore, ω_v is sensitive to the equivalent width detection threshold of the HIRES spectra. We are 93% complete to a 5σ rest-frame equivalent width detection threshold of 0.03 \AA for the full sample of 45 systems (see

Figure 3 from Paper I). To enforce uniform evaluation of the kinematic spread for the full sample, we omitted features with $W_r(\text{Mg II}) < 0.03 \text{ \AA}$ from the computation of ω_v . Six systems required this censorship step; they are footnoted in Table 1. The maximum change in ω_v from its uncensored value was a -20% difference, except for one of the absorbers (PKS 0454 + 039 at $z = 1.1532$), which was changed by a -40% difference.

To measure the kinematic “composition” of the low ionization gas, we use Voigt profile fitting. We use our own program, MINFIT (Churchill 1997), which performs a χ^2 minimization using the NETLIB-SLATEC routine DNLS1 (More 1978). In fully saturated profiles, the number of clouds is often underestimated by a factor of a few (Churchill 1997). A corollary is that the cloud column densities, b parameters, and velocities are correlative with the number of clouds. We return to this issue in § 4.2.

3. CHARACTERIZING Mg II ABSORBER PROPERTIES

We have constructed a subsample of 30 systems, Sample CA (CA = Cluster Analysis), in order to examine variations and possible trends between the absorption properties listed in Table 1. All Sample CA members have *measured* $W_r(\text{Ly}\alpha)$, $W_r(\text{Mg II})$, and ω_v and have *measurements of or limits on* Fe II and C IV. Systems with upper limits on $W_r(\text{Fe II})$ were included in the sample because these limits are already capable of demonstrating a paucity of Fe II absorption (only seven Sample CA systems have Fe II limits). Small $W_r(\text{Mg II})$ systems with upper limits on C IV were excluded from the sample because the limits were not always stringent. However, multiple cloud systems with limits on $W_r(\text{C IV})$ and larger $W_r(\text{Mg II})$ are included. The members of Sample CA are given in column nine of Table 1.

In Figure 1, we present three dimensional plots of (a) $W_r(\text{Mg II})$ vs. $W_r(\text{Ly}\alpha)$ vs. $W_r(\text{C IV})$, (b) $W_r(\text{Mg II})$ vs. $W_r(\text{Ly}\alpha)$ vs. $W_r(\text{Fe II})$, and (c) $W_r(\text{Mg II})$ vs. ω_v vs. $W_r(\text{C IV})$ for Sample CA. Note that distribution of equivalent widths are not random; there is a clear trend for $W_r(\text{Mg II})$ to increase with $W_r(\text{Ly}\alpha)$, for example. On the other hand, it is clear that there are significant spreads, or variations in the absorption strengths. In the case of $W_r(\text{Fe II})$, we see a very large range of values (Figure 1b) that trace $W_r(\text{Ly}\alpha)$, and to a lesser extent $W_r(\text{Mg II})$. $W_r(\text{C IV})$ exhibits a significant spread for a given $W_r(\text{Mg II})$ – $W_r(\text{Ly}\alpha)$ locus (Figure 1a). Moreover, note the groupings of $W_r(\text{Mg II})$, ω_v , and $W_r(\text{C IV})$ (Figure 1c).

From an empirical point of view, the qualitative appearance of groupings in Figure 1 would suggest that Mg II–selected systems can be further categorized (quantitatively) by their absorption properties. However, our sample is small, having only 30 data points, and it is not clear whether the apparent groupings would statistically be present in other “realizations” of the data⁶. This concern is best addressed by using a multivariate analysis in which all available absorption properties are incorporated simultaneously (multidimensional version of Figure 1 with one dimension for each property).

When the Ly α , Fe II, and C IV and Mg II kinematics are simultaneously considered, do we find various “classes” of Mg II absorbers? In other words, can we quantitatively describe both the variations and the trends by considering all the absorption line data presented in Table 1? To address these questions, we applied “Tree Clustering” and “ K -means Clustering” analysis

⁶Monte Carlo realizations of our sample could shed light on this issue if, and only if, we had *a priori* knowledge of the distribution functions for all the properties being studied.

to sample CA.

3.1. A Multivariate Analysis

Multivariate clustering analysis algorithms are designed to organize data of many variables into categories so that natural groupings of the data can be examined in a completely unbiased manner (i.e. no model is imposed upon the data). Full details of these techniques can be found elsewhere (e.g. Johnson & Wichern 1992; Babu & Feigelson 1996); below, we provide limited background material. We used the STATISTICA software package (www.statsoft.com).

3.1.1. Tree Cluster Analysis

In tree cluster analysis, the data occupy a multi-dimensional space, one dimension for each measured absorption property. Clustering algorithms compute the “distances” between each pair of points (absorbers) and then amalgamate them into clusters. We note that tree cluster analysis is not subject to significance testing because the result itself is the most significant solution under the assumption of no *a priori* hypothesis regarding the data.

The amalgamation process begins with each absorber in a unique class by itself and then proceeds by relaxing the criterion of uniqueness in subsequent steps. With each step, the algorithm amalgamates larger and larger clusters of increasingly dissimilar properties, until in the final step all absorbers are joined together in a single class. Graphically, clusters appear as distinct “branches” in a hierarchical tree, with similarities linked at nodes. We used Euclidean distances [i.e. $(\sum_i [x_i - y_i]^2)^{1/2}$] and Ward’s method (Ward 1963) for the amalgamation algorithm. Ward’s method minimizes the sum of squares of the distances between clusters. The combination of Euclidean distances and Ward’s amalgamation rule uses an analysis of variances approach for which $N(0, 1)$ standardization of the data is optimal. With this standardization, each variable is baselined and scaled to have a zero mean and unity standard deviation. $N(0, 1)$ standardization ensures that the distance between any pair of points in multidimensional space is not biased by a large dynamic range in one or more of the variables (dimensions).

3.1.2. *K*-means Clustering

In *K*-means clustering analysis, we begin with the assumption of a set number of clusters and the algorithm finds the most significant, or distinct, clusters possible. Starting with *K* random clusters, the algorithm moves points (absorbers) between clusters until both the variability within clusters is minimized and the variability between clusters is maximized. We find that $K = 5$ is the highest number of clusters allowed such that all clusters are considered significant, based upon MANOVA tests (Johnson & Wichern 1992; also see Mukherjee et al. 1998). For five clusters, the MANOVA probabilities, p , for accepting a result as valid, (i.e. representative of a unique population) are highly significant. We obtained $p < 10^{-5}$ for each cluster.

3.2. Results

In Figure 2, we present a dendrogram, the tree diagram showing the results of our cluster analysis. Along the bottom horizontal axis are the individual Mg II systems identified by quasar and absorber redshift. The vertical axis is the linkage distance, LD , the distance between clusters. The larger the value of LD

between two branches, the less related are the objects on each branch.

At $LD \sim 16$ there is a natural grouping into three clusters. These three clusters are *predominantly* distinguished by very strong Ly α [right branch, labeled “DLA/HI-rich”], weaker C IV [center branch, labeled “CIV-weak”], and intermediate to stronger C IV [left branch, labeled “CIV-strong”] absorption.

Further insight into the physical differences in the absorbers can be obtained if we adopt a “less significant” linkage distance. At $LD \sim 4$ there is a secondary grouping into six clusters. The CIV-strong and CIV-weak clusters have each been separated by variations in Mg II strengths and kinematics and the DLA/HI-Rich cluster has been separated by a spread in the Ly α strengths. However, we treat the DLA/HI-Rich systems as a single cluster because the MANOVA significance test from a *K*-means clustering analysis indicates that the further splitting of the DLA/HI-Rich cluster is not justified. On Figure 2, we have labeled each of these five clusters as “Classic”, “Double”, “Single/Weak”, “CIV deficient”, and “DLA/HI-Rich”.

It is in a diagram of the *K*-cluster means, Figure 3, that the properties distinguishing each cluster become apparent. Across the horizontal axis of Figure 3 are the absorption properties; from left to right they are the Mg II, Ly α , C IV, and Fe II absorption “strengths”, and the “strength” of the kinematic spread. Recall that the data have been $N(0, 1)$ standardized. Thus, for each given absorption property, the mean value for *all* systems is zero and the vertical axis is in units of standard deviations. Each cluster is represented by a different data point type: Classic (solid circle); Double (solid square); Single/Weak (open circle); CIV deficient (solid triangle); and DLA/HI-Rich (solid pentagon). These classes are also connected by unique line types (i.e. dash-dot, solid, etc.); it is important to not only compare a given property across clusters, but to compare how *all* properties are segregated by cluster. We now briefly discuss some distinguishing features of each absorber class.

3.2.1. Classic Systems

This class appears to have what might be thought of as “typical”, or non-extreme properties. As seen in Figure 3, this class is characterized by having Mg II, Ly α , Fe II, and C IV equivalent widths, and a kinematic spread within 0.5σ of the respective means for the overall sample.

We call these systems “Classic” because they can be thought to represent the most common type of Mg II absorber observable in earlier generation, low resolution surveys (e.g. Steidel & Sargent 1992; Lanzetta, Turnshek, & Wolfe 1987). To the sensitivities of these surveys, it was found that virtually all Mg II absorption-selected systems also had C IV absorption.

3.2.2. CIV “Deficient” Systems

The CIV-deficient systems have Mg II, Ly α , and Fe II properties identical to the Classics and constitute a similar fraction of the overall Mg II absorber population. Their distinguishing properties are significantly lower C IV absorption strengths.

3.2.3. Double Systems

The Doubles are set apart from the Classics by having at least twice the Mg II and C IV absorption strengths and Mg II kinematics. Since the mean Mg II strength for Doubles is in the same regime as of the DLA/HI-Rich systems, it is the C IV strengths and extreme Mg II kinematics that set this class apart from the others. Doubles also have Ly α and Fe II absorption

strengths that are systematically greater than those of the Classics.

3.2.4. Single/Weak Systems

The Single/Weak class is defined foremost by very small Mg II strengths and kinematics. In fact, with the exception of two systems, all are single, narrow clouds (often unresolved in the HIRES spectra).

The Single/Weak systems are underrepresented in Sample CA, mostly because seven of the systems in our database have no measured Ly α . If these seven systems were included with their C IV limits artificially treated as detections, the mean C IV for this class would drop to -1.1 (this being an upper limit) in the K -means cluster diagram (Figure 3). Thus, there is a spread in the distribution of C IV strengths associated with Single/Weak systems. The true mean Fe II is also probably lower than that shown on Figure 3 because the limits on Fe II in the HIRES spectra scatter about the measured mean. Thus, higher sensitivity spectra would reduce the mean Fe II for this class and could reveal a spread in Fe II strengths. Only for the Single/Weak class, for which many of the properties were below our detection thresholds, are the above issues pertinent.

3.2.5. DLA/HI-Rich Systems

The DLA/HI-Rich class has very strong Mg II, and extremely strong Ly α and Fe II, relative to the overall Mg II absorber population. They have C IV strengths below that of the Classics and Mg II kinematics typical of the Classics and C IV-deficient absorbers. Their Mg I and Fe II strengths are five to ten times greater than those of the typical Classic absorber. Unlike the elevated Ly α strengths, which are due to broad damping wings, the Mg I and Fe II strengths are driven by the line-of-sight kinematic spreads of the gas for multiple, saturated components. For the intermediate ionization species, Si II, Al II, C II and Si III, the strengths are somewhat greater than those of the Classics, on average. The higher ionization species, Si IV, N V and O VI (to the extent the latter two have been measured), have strengths consistent with those of the Classics absorbers.

3.3. Robustness of the Clustering Analysis

Two concerns regarding the clustering analysis are: (1) possible biasing due to an slight, but apparent, overabundance of absorbers with $W_r(\text{Mg II}) > 1.3 \text{ \AA}$, and (2) the exclusion of the “weak” systems for which only upper limits on the C IV equivalent widths were measured.

The systems with $W_r(\text{Mg II}) > 1.3 \text{ \AA}$ are all members of the DLA/HI-Rich class. Of these, four are bonified DLAs with $N(\text{HI}) \geq 2 \times 10^{20} \text{ cm}^{-2}$, whereas two have column densities below this classical threshold (i.e. they are HI-Rich systems). In an unbiased survey for $z < 1.65$ DLAs, using Mg II absorption as a selection method, Rao & Turnshek (1999) found that 14% of the Mg II systems with $W_r(\text{Mg II}) > 0.3 \text{ \AA}$ are DLAs. In our sample, 22 systems have $W_r(\text{Mg II}) > 0.3 \text{ \AA}$; thus, 18% of our sample is comprised of DLAs. This is not inconsistent with the unbiased results of Rao & Turnshek.

The presence of a DLA/HI-Rich class in our sample is not due to the slight bias (overabundance) of the larger $W_r(\text{Mg II})$; it is mostly defined by large HI and Fe II equivalent widths. In fact, one DLA has $W_r(\text{Mg II}) = 0.9 \text{ \AA}$ ($z = 0.5764$ toward Q 0117 + 213), and was classified as DLA/HI-Rich in

spite of the fact that this Mg II equivalent width is well below 1.3 \AA . In other words, even if the Mg II equivalent widths of the DLA/HI-Rich systems were quite small, the class would be unchanged in the cluster analysis due to the very strong HI and Fe II strengths. This is clearly shown in Figure 3.

To investigate whether membership in a given class (especially the Single/Weak class) may be sensitive to the inclusion of systems for which only an upper limit is available for $W_r(\text{C IV})$, we ran the cluster analysis including the four additional systems with information on Ly α (without regard to whether C IV was measured or an upper limit). In this analysis, the C IV upper limits were treated as measured values. The class memberships were unchanged for the original 30 systems. The added systems were classified as Single/Weak based upon their small $W_r(\text{Mg II})$ and narrow kinematics. This was expected, given the already large spread in $W_r(\text{C IV})$ for the Single/Weak class.

We thus conclude that the clustering results are robust; they are not affected by biases nor are they sensitive to changes in the sample.

3.4. Absorption Strengths

In Figure 4, we present the rest-frame equivalent widths (taken from Table 1 and from Tables 3 and 4 of Paper I) vs. $W_r(\text{Mg II})$. We have also included $W_r(\text{Ca II})$ vs. $W_r(\text{Mg II})$. The panels are ordered by increasing ionization potential from the upper left to the lower right and the data point types are the same as in Figure 3.

For the non-DLA/HI-Rich systems, note that the absorption strengths of the low ionization species Mg I, Fe II, Si II, Al II, and C II increase with increasing $W_r(\text{Mg II})$, indicating these species arise in the phase giving rise to the Mg II absorption. Overall, the higher ionization species Si IV and C IV exhibit more scatter, as quantified by the dispersion per observed range.

We caution that the classification scheme introduced above should not be taken to suggest that Mg II absorbers group into discretized classes. Discretization is a byproduct of clustering analysis. In fact, the distribution functions of the equivalent widths plotted in Figure 4 are characterized by single modes and decreasing tails⁷ As such, any single absorption property, viewed in this univariate fashion, is distributed continuously. However, from the perspective of a multivariate analysis, it is clear that *the overall properties of Mg II absorbers group in well defined regions of a “multi-dimensional space”*.

4. INFERRING IONIZATION CONDITIONS AND KINEMATICS

To examine the kinematic and ionization conditions, we define a new subsample, IC (IC = Ionization Conditions). Sample IC includes only those systems with (1) an Mg II equivalent width detection threshold less than or equal to 0.02 \AA , and (2) no unresolved saturation in at least four adjacent pixels (1.33 resolution elements) in the Mg II $\lambda 2796$ profile. These selection criteria enforce a high level of accuracy in the number of Voigt profile components, N_{cl} , and their column densities, velocities, and b parameters. Simulations of blended, multiple component Mg II profiles with these characteristics show that the distribution of Voigt profile parameters output from Voigt profile fitting is consistent (99% confidence) with those used to generate the profiles (Churchill 1997). Data with lower signal-to-noise ratios result in a slight paucity of Voigt profile com-

⁷The exceptions are $W_r(\text{Mg I})$, $W_r(\text{Fe II})$, and $W_r(\text{Ly } \alpha)$, which are bimodal due to the DLA/HI-Rich class. However, it is not clear if this bimodality is due to small numbers and/or is due to the relatively large number of DLAs in our sample.

ponents, and therefore (to compensate) the resulting components have column densities and b parameters that are too large. Profiles with severely saturated cores (e.g. DLA/HI–Rich absorbers) systematically have fewer Voigt profile components by a factor of three and have unconstrained column densities and b parameters. The equivalent width threshold criterion directly translates to a signal–to–noise ratio criterion of $S/N = 22$ per resolution element in the continuum. Sample IC membership is given in column nine of Table 1.

4.1. Ionization Conditions

4.1.1. Single/Weak Systems

Normally, it is difficult to interpret the ionization conditions based upon equivalent widths because simple curve of growth arguments are muddled by the possibility of unresolved saturation in multiple component absorption. However, these arguments *can* hold for the Single/Weak clouds.

As shown by Churchill et al. (1999a), under the assumption of photoionization, Single/Weak clouds with $W_r(\text{Mg II}) \leq 0.15 \text{ \AA}$, cannot give rise to $W_r(\text{C IV}) \geq 0.2 \text{ \AA}$ (see their Figure 12). The upper limit on $W_r(\text{C IV})$ is significantly more restrictive when Fe II is detected in the Mg II cloud (i.e. the cloud is constrained to have low ionization conditions). Based upon this analysis, we find that roughly half of the observed Single/Weak absorbers likely have multiple ionization phases, with C IV and some portion of the Ly α absorption arising in spatially distinct, higher ionization material. These findings are confirmed in a thorough study using CLOUDY (Ferland 1996) photoionization models tuned to the measured Mg II column densities and constrained by the full complement of ionization species and transitions covered in FOS spectra (Rigby et al. 1999)

4.1.2. Multicloud Systems

We now use photoionization modeling to investigate whether multiphase ionization can also be inferred for the multicloud Classic, C IV–deficient, and Double systems. We consider whether the measured C IV and/or Si IV absorption can or cannot all arise in the Mg II clouds, even under extreme assumptions about their ionization conditions. The following is based upon the methods employed by Churchill & Charlton (1999) in their study of the $z = 0.9276$ systems toward PG 1206 + 459.

We assumed that the Mg II clouds in a given system are in photoionization equilibrium and used CLOUDY (Ferland 1996) to model their ionization conditions. A Haardt & Madau (1996) extragalactic spectrum at $z = 1$ was used for the ionizing radiation. Based upon experiments with various single and extended starburst galaxy spectral energy distributions (Bruzual & Charlot 1993) with assumed high photon escape fractions, we determined that CLOUDY models involving Mg II, Fe II, Si IV, and C IV are not highly sensitive to the chosen spectrum for $z \sim 1$ (Churchill & Charlton 1999); thus our general conclusions are not sensitive to the assumed spectral energy distribution.

We obtained a predicted C IV and Si IV equivalent width for each system by tuning a CLOUDY model to the observed Mg II and Fe II column densities in each of its clouds. We then measured the absorption strengths in synthesized HIRES spectra using the velocities and b parameters thermally scaled from those measured for the Mg II clouds [see Churchill & Charlton (1999) for details.]

Since our goal is to infer if multiphase ionization structure

is possibly present in a given system, we have forced the models to yield the maximum amount of C IV and Si IV that can arise in the Mg II clouds. If a cloud has detected Fe II, then, for a given $[\alpha/\text{Fe}]$ abundance pattern under the assumption of negligible dust depletion, the Fe II and Mg II column densities uniquely determine the ionization parameter (the logarithm of the ratio of the number density of hydrogen ionizing photons to the number density of hydrogen), nearly independent of metallicity. The ionization parameter uniquely dictates the C IV and Si IV column densities in the clouds. Typical ionization parameters in the clouds with Fe II are -4 to -3 . We use a solar $[\alpha/\text{Fe}]$ abundance pattern, since this yields a higher ionization parameter for a given ratio of Mg II to Fe II column densities, and thus yields a maximized C IV and Si IV strength. If there is no detected Fe II for a cloud (either a limit or no coverage), then the ionization parameter is pushed to as high a value as possible without the cloud size exceeding 10 kpc. Typically, this occurs at an ionization parameter of ~ -1.9 . A solar metallicity was assumed for all clouds, again in order to maximize the predicted C IV and Si IV strengths (for a high metallicity cloud, the hydrogen column density required to give rise to the observed Mg II is smaller, and the ionization parameter can be pushed to a higher value). We did not apply any other constraints from the data (e.g. Si II, C II, etc.) than those described above.

In Figure 7, we present the predicted maximum equivalent widths vs. the observed equivalent widths for C IV (left panel) and Si IV (right panel). The mean error in the measured values is depicted by the open–box data point in the upper left of each panel. Diagonal lines demarcate those systems that are inferred to have multiphase ionization (lower right) from those that could be single phase. The maximum predicted C IV strength that can arise in photoionized Mg II clouds is more than 3σ short of the observed $W_r(\text{C IV})$ for a number of systems. Even two of the C IV–deficient systems are below the line. This implies that even though these particular systems have below average C IV absorption strengths, the C IV may still arise in a distinct, higher ionization phase and not in the Mg II clouds. For Si IV, it appears that fewer systems would require multiphase structure in this ionization species; Si IV likely resides in the Mg II clouds in a larger fraction of Mg II selected absorbers than does the C IV.

4.2. Mg II and C IV Kinematics

4.2.1. Number of Clouds

In Figure 6, we show these same absorption strengths vs. the number of clouds, or subcomponents, N_{cl} , obtained from Voigt profile decomposition. The data point types are the same as for Figure 4.

There is a strong correlation of $W_r(\text{Mg II})$ with N_{cl} , the number of Voigt profile components (also see Petitjean & Bergeron 1990). A linear least–squares fit, which we have drawn as a dotted line in Figure 6, yielded a slope of $0.069 \pm 0.005 \text{ \AA cloud}^{-1}$. Note that this relationship is likely resolution dependent. Also note that the fit is strongly influenced by the two Double systems with large N_{cl} .

We find that there is not as “linear” a dependence for $W_r(\text{Fe II})$ nor for $W_r(\text{C IV})$ with Mg II kinematics. There is, however, a tight correlation of $W_r(\text{Ly}\alpha)$ with the number of Mg II clouds. We obtained a linear least–squares fit (drawn as a dotted line) with slope $0.57 \pm 0.08 \text{ \AA cloud}^{-1}$. *The linear relationship for $W_r(\text{Mg II})$ vs. N_{cl} suggests that majority of neutral hydrogen equivalent width arises in the Mg II clouds*

themselves.

4.2.2. Mg II Kinematics

In Figure 5, the absorption strengths of Mg II, Fe II, Ly α , and CIV are plotted vs. the Mg II kinematic spread, ω_v . The data point types are the same as for Figure 4.

In Figure 5, the scatter in $W_r(\text{Mg II})$ arises because the Mg II equivalent width is dominated by the largest clouds, which are usually clustered in subgroups with velocity spreads less than $\sim 20 \text{ km s}^{-1}$ [see Figure 12 of Charlton & Churchill (1998)]. The kinematic spread, on the other hand, is sensitive to the presence of small $W_r(\text{Mg II})$ clouds with large velocities ($\omega_v \propto v^2$). The “limit” along the upper left of the data, shown as a dotted line, is due to saturation in the profile line cores; there is a maximum equivalent width for a given velocity spread when the profile is black bottomed. The “limit” along the lower right is due to detection sensitivity; for the signal-to-noise ratios of the sample, there is a minimum detectable $W_r(\text{Mg II})$ for a given velocity spread. Higher quality data would be required to determine if there is an actual paucity of systems with large kinematic spreads and extremely weak Mg II absorption.

The strong correlation between $W_r(\text{CIV})$ and ω_v has previously been discussed by Churchill et al. (1999b). The correlation is driven by the three Double systems ($z = 0.8514$ toward Q 0002 + 051, $z = 0.9110$ toward PKS 0823 – 223, and $z = 0.9276$ toward PG 1206 + 459) and the two kinematically extreme Classic systems ($z = 1.3250$ toward PG 0117 + 213 and $z = 0.7908$ toward PKS 2145 + 067), which all have $\omega_v \geq 75 \text{ km s}^{-1}$. We have drawn in the maximum-likelihood linear fit to the data, which has slope $15.4 \pm 0.2 \text{ m\AA (km s}^{-1})^{-1}$. More data on Double systems at intermediate redshifts, selected by $W_r(\text{Mg II}) > 0.6 \text{ \AA}$, would be useful for determining how tight the relationship between $W_r(\text{CIV})$ and Mg II kinematics remains for the largest kinematic spreads.

Three of the five Classic systems above the correlation line are from the lowest signal-to-noise spectra; there could be missed, small equivalent width components resulting in a small ω_v . Even so, there is a significant scatter in $W_r(\text{CIV})$ at a given ω_v for $\omega_v \leq 60 \text{ km s}^{-1}$. The Single/Weak systems have $W_r(\text{CIV}) \simeq 0.5 \text{ \AA}$ and $\omega_v \simeq 5 \text{ km s}^{-1}$, whereas the CIV-deficient systems have $W_r(\text{CIV}) \leq 0.2 \text{ \AA}$ and $\omega_v \simeq 45 \text{ km s}^{-1}$.

4.2.3. CIV Kinematics

In Figure 8 we display the suite of CIV doublets featured in FOS spectra (we exclude ground based data; see Paper I) that are not blended with other transitions. The velocity window for the CIV doublets is 2000 km s^{-1} . Above each doublet member are ticks giving the velocities of the Mg II Voigt profile components. The Mg II $\lambda 2796$ profiles are also shown with the Voigt profile models superimposed on the data, which are ordered by increasing kinematic spread, ω_v . The velocity window for the Mg II data is 600 km s^{-1} .

To demonstrate which profiles are resolved, and to quantify the degree to which they are resolved, we fit the individual CIV members with single Gaussians while holding the width constant at the value of the instrumental spread function, $\sigma = 98 \text{ km s}^{-1}$. We have superimposed these *unresolved fits* on the CIV $\lambda\lambda 1548, 1550$ profiles. We note that several of the spectra were obtained prior to the refurbishing mission in which COSTAR was installed. For “large” aperture acquisition modes

(1" slit), the instrumental spread function of the pre-COSTAR instrument has extended wings. PKS 0454 – 220 is the only object acquired in this mode; thus, the unresolved fit to the $z = 0.4744$ system should be viewed with some discretion. Several of the unresolved fits are consistent with the CIV data, suggesting that the adopted instrumental spread function accurately represents the pre-COSTAR and post-COSTAR instrument for the smaller apertures modes.

We computed the quantity,

$$F_r = \frac{W(\text{measured}) - W(\text{unresolved})}{W(\text{measured})}, \quad (2)$$

where $W(\text{measured})$ is the measured CIV equivalent width adopted for Table 1, and $W(\text{unresolved})$ is the CIV equivalent width from the unresolved fits. Thus, F_r measures the fraction of the integrated flux due to resolved velocity structure in the CIV doublet. We have noted the F_r value and its 1σ uncertainty for each CIV profile in Figure 8. There is a 3σ correlation between F_r and ω_v . *We have thus demonstrated that the tight $W_r(\text{CIV})$ vs. ω_v correlation is due to resolved velocity structure in the CIV absorbing gas.*

Velocity structure is not unexpected. Observed at higher resolution, CIV profiles from Milky Way halo gas exhibit velocity structure over a $\sim 200 \text{ km s}^{-1}$ spread, though the components are typically blended together (Sembach et al. 1999b). For higher redshift galaxies, the CIV profiles also show distinct velocity structure (Petitjean & Bergeron 1994) with velocity spreads up to 200 km s^{-1} . In Figure 9, we present an example of a kinematically complex CIV doublet ($\sim 9 \text{ km s}^{-1}$ resolution) and two Fe II transitions (Mg II was not covered) for the damped Ly α absorber at $z = 1.7763$ toward Q1331+170⁸. The ticks above the CIV profiles were obtained by a crude Voigt profile fit to the strongest components to parameterize the kinematics; we used this fit to synthesize the CIV doublet as it would be observed with FOS resolution and pixel sampling (infinite signal-to-noise ratio). This is shown in the separate, bottom panel of Figure 9, with the CIV $\lambda 1548$ and $\lambda 1551$ component ticks above the continuum (not the Mg II ticks as in Figure 8). An unresolved fit is superimposed on the synthetic FOS doublet for which we measured $F_r = 0.27 \pm 0.02$. This value is comparable to F_r for the $z = 0.5505$ system toward Q 1241 + 174 and the $z = 0.9110$ double system toward PG 0823 – 223.

In cases where the Mg II profiles are highly asymmetric, it appears that the CIV profiles exhibit similar asymmetry in the same sense. That is, the flux discrepancies between the unresolved fits and the CIV profiles are aligned in velocity with the kinematic outliers seen in Mg II. Since we have demonstrated that, in most cases, the CIV does not arise in the same phase as the Mg II clouds (see § 4.1.2), *we infer that the CIV often arises in a physically distinct structure from the Mg II, but is aligned kinematically with the Mg II.*

5. ABSORPTION-GALAXY PROPERTIES

We tested for correlations between the galaxy properties and all the absorption line data presented in Paper I, including all possible combinations of equivalent width ratios. We performed Kendall and Spearman non-parametric rank correlation tests using the program ASURV (LaValley, Isobe, & Feigelson 1992). The ASURV algorithm provides for measurements that are either upper or lower limits.

⁸Interestingly, this DLA has $W_r(\text{CIV}) = 1.63 \text{ \AA}$, twice that of the DLA/HI-Rich systems in our lower redshift sample. It has $W_r(\text{Mg II}) = 1.3 \text{ \AA}$ (Steidel & Sargent 1992)

Out of 114 tests performed, seven resulted in correlations above the 2.5σ level⁹; these are: $W_r(\text{Mg II})$, Mg II doublet ratio, and $W_r(\text{Si IV})/W_r(\text{C IV})$ vs. impact parameter; $W_r(\text{C II})$ and $W_r(\text{Mg II})$ vs. M_K ; and $W_r(\text{Ly } \alpha)/W_r(\text{C IV})$ and $W_r(\text{Si II})/W_r(\text{Si III})$ vs. $B - K$. When DLA/HI-Rich systems were removed from the sample, the significance levels dropped slightly below 2.0σ . No test resulted in a correlation at a 3.0σ or greater significance level.

5.1. Global Ionization and Density Structure?

In Figure 10 we present plots of the absorption properties used in our multivariate analysis, ω_v , $W_r(\text{Mg II})$, $W_r(\text{Fe II})$, $W_r(\text{Ly } \alpha)$, and $W_r(\text{C IV})$, vs. host galaxy properties.

$W_r(\text{Mg II})$ is anti-correlated with impact parameter (decreases with galactocentric distance) with a 2.7σ significance and is correlated with M_K (increases with decreasing luminosity), also with a 2.7σ significance. Both these trends arise because DLAs, which give rise to the largest $W_r(\text{Mg II})$, are often observed at low impact parameters and often have low luminosities ($M_K > -24$).

The $W_r(\text{C IV})$ vs. K luminosity relationship can provide a test for halo models in which a virialized hot phase ($T \sim 10^6$ K) pressure confines the low ionization phase (e.g. Mo & Miralda-Escudé 1996). These models predict an anticorrelation between $W_r(\text{C IV})$ and galaxy mass (i.e. K luminosity); C IV is predicted to be enhanced in smaller, lower mass galaxies, which have low gas pressures in their halos. As seen in Figure 10, there is a visual, yet not statistically significant, trend for the most massive galaxies to have smaller $W_r(\text{C IV})$ in our small sample. This is driven by the high luminosity [and very red; see $W_r(\text{C IV})$ vs. $B - K$] C IV-deficient systems.

In Figure 11, we have plotted the equivalent width ratios of Si IV to C IV, Ly α to C IV, Ly α to Mg II, Fe II to C IV, and the C IV and Mg II doublet ratios vs. impact parameter. We have selected combinations only of the gas properties used in our multivariate analysis, with the exception of the ratio $W_r(\text{Si IV})/W_r(\text{C IV})$. This ratio is anticorrelated with impact parameter at the 2.8σ level when all galaxies are included and at the 2.1σ level when DLA/HI-Rich systems are excluded. If this trend were to hold for a larger sample, it would be consistent with the scenario in which halo gas is photoionized by the extragalactic UV background flux resulting in an increasing ionization level with increasing galactocentric distance (see Savage, Sembach, & Lu 1997).

The Mg II doublet ratio is correlated with impact parameter at the 2.7σ significance level. This reflects the fact that the gas tends to become optically thin at larger galactocentric distances, where $W_r(\text{Mg II})$ is systematically smaller. Again, the DLAs dominate the trend.

The ratio $W_r(\text{Ly } \alpha)/W_r(\text{Mg II})$ is not correlated with impact parameter when all galaxies in the sample are included. However, when the DLA/HI-Rich systems are excluded a 2.5σ level correlation is observed. This is governed by the general decrease in Mg II equivalent widths with impact parameter, since Ly α shows no trend with impact parameter (when DLA/HI-Rich systems are excluded). This particular trend is difficult to interpret because of the very different curve of growth behavior for Mg II and Ly α . It is not possible to address the possibility of a metallicity or ionization gradient. The location of the Lyman limit break was covered for only six of the galaxies and was detected for all six, sampling impact param-

eters from 10 to 40 kpc.

5.2. Ionization Conditions and Colors

In Figure 12, we have plotted the C IV to Mg II, Ly α to C IV, and Ly α to Mg II equivalent width ratios vs. host galaxy $B - K$ color. Both $W_r(\text{Ly } \alpha)/W_r(\text{C IV})$ and $W_r(\text{Ly } \alpha)/W_r(\text{Mg II})$ are correlated with $B - K$ at a 2.6σ significance level. This trend in our small sample is governed by both the DLA/HI-Rich systems and the C IV-deficient systems being associated with redder galaxies.

5.3. Correlation Test: Overall Results

The degree of scatter in the absorption properties presented here are similar to that found by Churchill et al. (1996) for the Mg II absorption properties only. None of the presented absorption properties correlated with the galaxy properties at a *high* significance level. This is not to say that definite trends, or even statistically significant correlations, do not exist. The large scatter in the properties signifies large local variations from line of sight to line of sight through the galaxies; however, even with our small sample, we have uncovered some suggestive global trends.

We also find that the inclusion or exclusion of DLA/HI-Rich systems in any given test significantly alters the statistics. The host galaxies of DLAs are seen to have a wide range of luminosities, morphologies, colors, and surface brightnesses (e.g. Le Brun et al. 1997; Rao & Turnshek 1998), and do not represent a homogenous population, despite the fairly homogeneous absorption properties by which they are selected.

6. DISCUSSION

We reemphasize that a taxonomic scheme based upon a multivariate clustering analysis will, by its very nature, result in a discretization of what may actually be a continuum of properties. Nonetheless, if we adopt the clustering analysis results at face value (see § 3.2) and segregate the wide variety of Mg II absorber properties into individual “classes”, we may be able to find order in an otherwise complex array of gas properties and kinematics. The hope is to gain further insights into defining distinctive or “characteristic” properties of Mg II absorbers and to understanding the galactic processes that give rise to the observed range of these “characteristics”.

What follows is primarily a speculative discussion, given the fact that there is still very little data upon which inferences can be based.

6.1. Classic vs. C IV-deficient Systems

The existence of C IV-deficient systems with $W_r(\text{C IV}) \leq 0.15 \text{ \AA}$, which have kinematics similar to the Classics, indicates that the connection between C IV absorption and Mg II kinematics does not operate the same in all galaxies (or at all locations in galaxies).

There are only three C IV-deficient systems with measured galaxy properties ($z = 0.4297$ toward PKS 2128 - 123, $z = 0.6601$ toward Q 1317 + 277, and $z = 0.7291$ toward PG 0117 + 213). The host galaxies of these three systems are reddish ($B - K = 3.3, 3.8, \text{ and } 4.0$) and are among the more luminous ($M_K = -24.7, -25.7, \text{ and } -26.3$). Also, they are probed at large impact parameters ($D = 32, 38, \text{ and } 36 h^{-1} \text{ kpc}$), respectively (see Figure 10). The redder colors and large luminosities would suggest massive, early-type galaxies.

⁹For 114 correlations tests, only one test should result in a 2.5σ or greater significance level at random.

Based upon *HST* images of the $z = 0.6601$ and $z = 0.7291$ absorbers (Steidel 1998), we roughly (visually) classify them to be an edge-on S0 galaxy (probed on its minor axis) and a face-on Sba galaxy, respectively.

Despite small numbers, these relatively high masses, early-type morphologies, and large impact parameters may be a clue to the observed spread in $W_r(\text{CIV})$ for a given MgII absorption profile type. Semianalytical models of pressure confined gaseous halos predict smaller CIV strengths in more massive galaxies (e.g. Mo & Miralda-Escudé 1996), and such a trend is not inconsistent with our data. The weak CIV cannot simply be due to the line of sight through the galaxy, because some Classics at large impact parameters have very strong CIV strengths. Also, based upon cross-sectional arguments from the number of CIV absorbers per unit redshift (Steidel 1993) and upon the expected lower pressures and gas densities at larger galactocentric distances (Mo & Miralda-Escudé 1996), it is expected that CIV absorption would be strong at large impact parameters.

Perhaps strong CIV is expected in regions of relatively pronounced star formation, which would be consistent with CIV-deficient absorbers being associated with earlier-type galaxies. Alternatively, in CIV-deficient absorbers, the CIV could be ionized away due to collisional processes, such as with the intragroup medium scenario proposed by Mulchaey et al. (1996). If so, strong OVI absorption would be predicted; unfortunately, we cannot address OVI absorption for the CIV-deficient systems [only one is “measured” to have an unrestricted upper limit on $W_r(\text{OVI})$]. A further possibility is that galaxies with extended X-ray emission, usually early-type galaxies (e.g. Mathews & Brighenti 1998), may preferentially be CIV- and OVI-deficient because of the extremely hot environment. If so, the MgII absorbing gas would necessarily arise in HI gas, which is of external origin for ellipticals from galaxy mergings (Knapp, Turner, & Cunniffe 1985; van Gorkom 1992) and is sometimes found to be in disk-like structures extending 5 to 10 times the optical radii in “dust-lane” elliptical galaxies (e.g. Morganti, Oosterloo, & Tsvetanov 1998). Thus, one might hypothesize that MgII absorption associated with elliptical galaxies arises preferentially in post-merger ellipticals.

6.2. Classic vs. Double Systems

There are at least two obvious explanations for the Double systems; they might be two Classic systems clustered in line-of-sight velocity (bound or unbound), or a primary galaxy and a satellite (e.g. possible an interacting LMC-like object).

The three Double systems in our sample have the largest $W_r(\text{CIV})$, which are consistent with that of two typical Classic systems. Alternatively, they could arise in a primary galaxy either undergoing a minor merger or residing in a group with several minor galaxies. Using the Local Group as a model and applying the simple cross-sectional dependence for $W_r(\text{MgII})$ with galaxy luminosity (Steidel 1995; also see McLin, Giroux, & Stocke 1998), we estimated the probability of intercepting a “double” absorber for a random line of sight passing through the Milky Way (line-of-sight kinematics were not considered). We found a 25% chance of intercepting both the LMC and the Milky Way, and a 5% chance of intercepting both the SMC and the Milky Way. All other galaxies in the Local Group have negligible probabilities of being intercepted for a line of sight passing within 50 kpc of the Milky Way.

An alternative scenario is that Double systems are otherwise typical Classic systems, but for the interception of kinematic outlier clouds, either due to infalling or ejected “high velocity”

gas. This picture would naturally invoke elevated star formation to explain the large $W_r(\text{CIV})$ in Doubles and, possibly, the correlation between $W_r(\text{CIV})$ and MgII kinematics. Infalling material can enhance star formation (Hummel et al. 1990; Lutz 1992; Hernquist & Mihos 1995; Hibbard & van Gorkom 1996), which can provide the energetics to support a multiphase halo (Dahlem 1998) with strong CIV absorption [i.e., as with the Galaxy (Savage et al. 1997)]. Consistent with this scenario would be that the bluest galaxies would preferentially be associated with Double systems. Only one Double system has measured galaxy properties ($z = 0.8519$ toward Q 0002+051), and we note that its color ($B - K = 2.9$) is among the bluest in the sample, consistent with a star forming object. An *HST* image (Steidel 1998) reveals the galaxy to be compact with a spherical, featureless morphology (no evidence for merging).

6.3. Classic vs. DLA/HI-Rich

Though the Classic MgII systems are well understood to select normal, bright galaxies (Steidel et al. 1994), the DLA/ systems are seen to select [based upon $N(\text{HI}) \geq 2 \times 10^{20} \text{ cm}^{-2}$] an eclectic population of low luminosity, low surface brightness, and dwarf galaxies (Le Brun et al. 1997; Rao & Turnshek 1998, 1999). This might suggest that not all classes of MgII absorber have a systematic connection with galaxy type or galaxy properties.

What is interesting, however, is that the MgII kinematic spreads for DLA/HI-Rich systems are tightly clustered around $\sim 60 \text{ km s}^{-1}$, have no weak, kinematic outlier clouds, and have intermediate to weak CIV absorption strengths. This is in contrast to those at redshifts 2–3, where *strongly* absorbing, higher velocity outlying clouds and often “double” profiles are characteristic of low ionization DLA profiles (Lu et al. 1996).

Whatever physical process or environment gives rise to kinematic outlying MgII clouds and strong CIV, it is apparently not acting in intermediate redshift DLA/HI-Rich systems. Alternatively, these trends could be due to selection effects of sightlines through HI-rich environments, which implies a line-of-sight dependency for absorber class.

6.4. Absorber Class Evolution?

We have shown that there is a significant correlation between $W_r(\text{CIV})$ and the MgII kinematic spread. But, exactly how do the MgII kinematics vary with $W_r(\text{CIV})$ for a given $W_r(\text{MgII})$? In Figure 13, we have plotted the MgII $\lambda 2796$ profiles from our HIRES/Keck spectra in the approximate locations they occupy in the $W_r(\text{CIV})$ – $W_r(\text{MgII})$ plane. Based upon this schematic, we have an impression of how the kinematic “complexity” of the absorption profile relates to both the MgII and CIV absorption strengths. Roughly, each of the five classes obtained from our multivariate analysis falls in a well defined region, which we have marked to guide the reader. Note that, in general, the CIV strength is largest when the kinematic “complexity” is the greatest; CIV absorption appears to have no direct connection with the optical depth of the strongest MgII component, nor with the total number of Voigt profile components. Most remarkably, it would appear that the *gross* characteristics of the MgII kinematics can be predicted simply based upon the absorber’s location on the $W_r(\text{CIV})$ – $W_r(\text{MgII})$ plane.

Since the distribution of MgII equivalent widths evolves with redshift (Steidel & Sargent 1992), and this must be reflected in the MgII kinematics as well, it seems reasonable to assume that

evolution should be discernable on the $W_r(\text{CIV})-W_r(\text{Mg II})$ plane.

There are at least two possible types of evolution of absorber classes: (1) the number density per unit redshift of a given class could evolve, either diminishing with or increasing with time, and/or (2) any absorber in a given class could evolve into another class. The former is systematic and would indicate a global, cosmic evolution, which might imply the existence of absorber classes not seen in our intermediate redshift sample. The latter form of evolution would be stochastically related to the processes occurring in galaxies and their environs.

We present the observational $W_r(\text{CIV})-W_r(\text{Mg II})$ plane in Figure 14. The intermediate redshift data (taken from this study) have small, filled circle data points. We have included lower and higher redshifts data from the literature, which we have listed in Table 3. The higher redshift absorbers ($1.2 \leq z \leq 2.1$) are taken from Bergeron & Boissé (1984), Boissé & Bergeron (1985), Lanzetta et al. (1987), and Steidel & Sargent (1992) [six-pointed stars]. The lower redshift points ($0.1 \leq z \leq 0.6$) are taken from Bergeron et al. (1994) [downward pointing, open triangles], and the $z \simeq 0$ data¹⁰ are taken from Bowen et al. (1995, 1996), Jannuzi et al. (1998), and Bowen (1999, private communication) [open diamonds]. There are four extraordinary systems listed in Table 3 that have $W_r(\text{Mg II})$ ranging from ~ 4 to $\sim 7 \text{ \AA}$. These have not been presented in Figure 14.

Three points from Figure 14 are that (1) there are absorbers in the higher, lower, and $z \simeq 0$ redshift samples with CIV and Mg II strengths typical of each of the five classes found in our clustering analysis of the intermediate redshift systems; (2) there are both higher and $z \simeq 0$ redshift absorbers occupying regions of the $W_r(\text{CIV})-W_r(\text{Mg II})$ that are not represented in our intermediate redshift sample; and (3) as with the intermediate redshift systems, the higher redshift systems exhibit a large range of $W_r(\text{CIV})$ for a given $W_r(\text{Mg II})$. Though there is no suggestion for such a spread in the lower redshift systems, there are too few measurements to characterize the spread in $W_r(\text{CIV})$ values.

Given the fairly systematic dependence of kinematics in the $W_r(\text{CIV})-W_r(\text{Mg II})$ plane, we can infer that the Mg II kinematics of the lower and higher redshift systems that occupy locations consistent with a given absorber class are likely to be similar to that class' kinematics.

The higher redshift systems with $W_r(\text{Mg II}) > 2 \text{ \AA}$, are a class of absorber not present in our sample. Note the large spread in $W_r(\text{CIV})$ for these systems, which would suggest that some are ‘‘CIV deficient’’. This may be indicative that the physical processes giving rise to the range of $W_r(\text{CIV})$ in intermediate redshift systems are also occurring in these $W_r(\text{Mg II}) > 2 \text{ \AA}$, higher redshift systems.

In Figure 15, we present the HIRES/Keck Mg II $\lambda 2796$ profiles of four $z \geq 1$ Mg II systems with $W_r(\text{Mg II}) > 2.0 \text{ \AA}$. Note that the profiles are optically thick with virtually unity doublet ratio over a the full velocity span, which is typically 250 km s^{-1} or greater. We also show the $z \simeq 0$ Mg II profile measured in the spectrum of SN 1993J in M81 using the GHRS on *HST* (Bowen et al. 1995; spectrum provided courtesy of Dr. D. Bowen). In comparison to the smaller equivalent width, intermediate redshift absorbers, the Mg II kinematics and absorption strengths of these $W_r(\text{Mg II}) > 2 \text{ \AA}$ systems are clearly unique, exhibit-

ing ‘‘double’’ black-bottomed profiles.

Of the systems shown in Figure 15, only the $z = 1.7945$ system toward B2 1225 + 317 is represented on Figure 14. Though the CIV strengths of the other systems shown in Figure 15 are unmeasured or unpublished, it is clear that these systems constitute their own unique ‘‘class’’ (with respect to the five classes found in our clustering analysis). As shown in Figure 15, the Mg II kinematics are suggestive of ‘‘double-DLAs’’, and, in fact, the $z = 1.7945$ system toward B2 1225 + 317 is a DLA (Bechtold, Green, & York 1987). In high quality data, ‘‘Double-DLAs’’ might be expected to have slightly asymmetric damping wings, reflecting the different column densities in the two systems.

Steidel & Sargent (1992) found that the number density of these large equivalent systems decreases with redshift over the range $0.3 \leq z \leq 2.2$ (the full range over which the Mg II doublet is observable from the ground). Based upon the SN 1993J spectrum of M81 and the Galaxy in absorption (the line of sight passes through half the disk and halo of M81, half the disk and halo of the Galaxy, and through ‘‘intergalactic’’ material apparently from the strong dwarf-galaxy interactions taking place with both galaxies), one possibility is that these systems arise from two galaxies with low impact parameters that happen to have a line-of-sight superposition.

For this scenario to be consistent with the Mg II absorber evolution, the number of galaxy pairs would need to decrease in step with the evolution of the absorbers themselves over the same redshift regime. In fact, over the redshift interval $1 \leq z \leq 2$, it is seen that the galaxy pair fraction, where pairs are defined to have projected separations less than 20 kpc, evolves proportional to $(1+z)^p$, with $2 \leq p \leq 4$ (Neuschaefer et al. 1997, and references therein). Le Fevre et al. (1999) found a similar, better constrained result with $p = 2.7 \pm 0.6$ for $0 \leq z \leq 1$. These compare well with $p = 2.2 \pm 0.7$ for Mg II absorbers with $W_r > 1.0 \text{ \AA}$ (Steidel & Sargent 1992; the evolution is probably stronger for those with $W_r > 2.0 \text{ \AA}$).

As such, galaxy pair evolution remains a plausible scenario as a contribution to the evolution of large equivalent width, higher redshift Mg II absorbers and the class we loosely have called ‘‘Double-DLAs’’. We note, however, that outflows from very luminous, star bursting galaxies at these high redshifts could also account for some of these ‘‘super’’ systems, since the low ionization gas can be very prominent in absorption (Pettini et al. 1999).

7. SUMMARY

We have performed a multivariate analysis of the absorption strengths and kinematics of Mg II and the absorption strengths of Fe II, Ly α , and CIV for a sample of 45 Mg II absorption-selected systems. Descriptions of the survey and analysis of the data used herein have been presented in Churchill et al. (1997, 1999a) and in Paper I. The multivariate analysis was performed using the STATISTICA package (www.statsoft.com). We applied both a ‘‘Tree Clustering’’ and ‘‘K-means Clustering’’ analysis to the 30 systems in Sample CA from the data listed in Table 1.

We have also compared the low, intermediate, and high ionization absorption properties of 16 systems with the B and K luminosities, $B-K$ colors, and impact parameters of their host

¹⁰We note that the $z \simeq 0$ sample is small and is selected based upon a bright, background quasar having a small projected separation from a nearby galaxy, as opposed to being Mg II-absorption selected (Bowen et al. 1995); this may have introduced a bias, possibly related to impact parameter distribution, as compared to the higher redshift data.

galaxies. The full complement of absorption line data was taken from Paper I. The galaxy properties, listed in Table 2, are taken from the survey of Steidel et al. (1994) and the previous studies of Churchill et al. (1996) and Steidel et al. (1997). We tested for absorption–galaxy property correlations using Kendall and Spearman non–parametric rank correlation indicators as implemented with the program ASURV (LaValley, Isobe, & Feigelson 1992), which incorporates upper limits on the data.

The main results are summarized as follows:

1. The clustering analysis revealed that there is a wide range of properties for Mg II–selected absorbers and that these can be categorized into three *main* types (Figure 2). Based upon strong $W_r(\text{Ly}\alpha)$ and $W_r(\text{FeII})$, there is the class of DLA/HI–Rich Mg II absorbers. For the remaining systems, there is a spread in the CIV strengths for a given $W_r(\text{MgII})$ that gives rise to ‘CIV–weak’ and ‘CIV–strong’ systems.

2. The CIV–weak class separates into the Single/Weak and the CIV–deficient classes (Figures 2 and 3). Single/Weak systems are characterized by a single unresolved Mg II absorption line with $W_r(\text{MgII}) \leq 0.15 \text{ \AA}$, a velocity spread of $\omega_v \leq 6 \text{ km s}^{-1}$, and a range of CIV strengths, but with $W_r(\text{CIV})$ no greater than $\sim 0.5 \text{ \AA}$ (in our sample). The Mg II strengths and kinematics are the dominant properties in distinguishing them as a separate class. CIV–deficient systems have multiple Voigt profile components, $N_{cl} > 1$, a range of kinematic spreads, $15 \leq \omega_v \leq 45 \text{ km s}^{-1}$, and $W_r(\text{CIV})$ no stronger than 0.4 \AA . The CIV strength, and to a lesser degree the Mg II kinematics, are the dominant properties distinguishing this as a CIV–weak class.

3. The CIV–strong class separates into the Classics and the Doubles (Figures 2 and 3). Classic systems, like the CIV–deficient systems, have multiple Voigt profile components, and a similar, but slightly larger, range of kinematic spread. The CIV strengths, on the other hand, are greater than 0.4 \AA . Separate from the Classics are the Doubles, which are characterized by roughly twice the number of Voigt profile components, N_{cl} , twice the CIV strength, and twice the Mg II kinematic spread, as compared to the Classics.

4. The Mg II, and Ly α strengths are tightly correlated with the number of Mg II Voigt profile components, N_{cl} (see Figure 6). The tight correlation between $W_r(\text{Ly}\alpha)$ and N_{cl} implies that the majority of the neutral hydrogen is arising in the phase giving rise to the Mg II absorption. In single cloud, $N_{cl} = 1$, systems (the Single/Weak class), $W_r(\text{Ly}\alpha)$ ranges from $0.2\text{--}1.2 \text{ \AA}$ and $W_r(\text{CIV})$ ranges from less than 0.15 to 0.7 \AA , suggesting a range of metallicities and/or ionization conditions in this class of object.

5. There is a highly significant correlation between $W_r(\text{CIV})$ and ω_v (see Figure 5; also see Churchill et al. 1999b). This correlation is driven by the five absorbers (two Classics and three Doubles) with the largest ω_v . For $\omega_v \leq 60 \text{ km s}^{-1}$ there is a $\sim 1 \text{ \AA}$ spread in $W_r(\text{CIV})$, due to the CIV–deficient systems and the Single/Weak systems with larger $W_r(\text{CIV})/W_r(\text{MgII})$. More systems with $\omega_v \geq 80 \text{ km s}^{-1}$ are needed in order to determine if all ‘kinematically active’ Mg II absorbers have such strong CIV.

6. Assuming the Mg II clouds are in photoionization equilibrium, we showed that in many systems a substantial fraction of the CIV absorption is arising in a separate phase from the Mg II (see Figure 7). We also showed that some fraction of the systems likely have Si IV in a separate phase from the Mg II. The FOS profiles of the larger CIV absorbers (Classics with large

CIV and Doubles) are resolved due to the kinematic spread, or velocity structure, of the CIV phase. A quantity expressing the degree to which the profiles are resolved, F_r , correlates at the 99.99% confidence level with the Mg II kinematic spread. Furthermore, there is a clear impression that the asymmetries in the resolved CIV profiles trace the Mg II kinematics. The above facts lead us to suggest that, often, some of the CIV arises in a physically distinct phase from the Mg II gas, but is kinematically clustered with the Mg II clouds.

7. For our small sample of 16 galaxies, we find no significant trends (greater than 3σ) of CIV and Ly α , or their ratios with each other and with Mg II, with host galaxy B and K luminosities, $B - K$ colors, and impact parameters. DLA/HI–Rich systems, which have systematically smaller impact parameters and redder colors, significantly affect the outcome of correlation tests. The CIV and Ly α absorption properties do not smoothly depend upon global galaxy properties. At 2.8σ , we find that $W_r(\text{SiIV})/W_r(\text{CIV})$ decreases with impact parameter, which could be interpreted as very tentative evidence for a global galactocentric ionization/density gradient (see Figure 11). The available data also show marginal trends for redder galaxies to have lower ionization conditions (Figure 12). This is *suggestive* that CIV phases may be systematically smaller in the redder galaxies.

8. We found that the Mg II kinematics of a given absorber is related to its location in the $W_r(\text{CIV})\text{--}W_r(\text{MgII})$ plane. In a comparison of our intermediate redshift ($0.4 \leq z \leq 1.4$) with published low redshift ($0 \leq z \leq 0.6$) and high redshift ($1.2 \leq z \leq 2.1$) samples, we found evidence for redshift evolution in the $W_r(\text{CIV})\text{--}W_r(\text{MgII})$ plane. This implies that other ‘classes’ of absorbers are present at high redshift, possibly including a ‘Double DLA/HI–Rich’ class. There is also a group of ‘super’ Mg II systems at $z \sim 2$ that have a large range of $W_r(\text{CIV})$ values. We discussed a scenario in which the evolution of these strongest Mg II absorbers could be due to the evolution of the number of galaxy pairs and/or accreting LMC–like satellite galaxies.

7.1. Further Ruminations

In general, the observed range of Mg II kinematics and CIV absorption strengths could be due to a number of factors. These include global differences in gaseous conditions related to environment (i.e. group or isolated galaxies) or galaxy morphology, local variations dominated by passage through different parts of host galaxies (e.g. halos, outer disks, spiral arms, etc.), or small scale fluctuations in galactic interstellar and halo structures. An additional important issue is whether characteristic absorption properties might be tied to the evolutionary stage of the host galaxy. This would imply that a given host galaxy may not always be of the same ‘absorber class’ throughout its evolution.

At higher redshifts ($z \geq 2$), galaxy–galaxy interactions were more common and no doubt played an important role in the kinematics and multiphase ionization conditions in many Mg II absorbers (e.g. Carilli & van Gorkom 1992; Bowen & Blades 1993; Bowen et al. 1995). A local analogue is seen in absorption associated with M61, a nearly face–on, later–type galaxy with enhanced star formation. The Mg II velocity spread is $\sim 300 \text{ km s}^{-1}$ at an impact parameter 21 kpc and there are two nearby galaxies (Bowen et al. 1996).

Since it is the kinematic *complexity* and spread and not the total amount of the Mg II that appears to be the important property for predicting the CIV strength in $z \sim 1$ galaxies, it is not unreasonable to conjecture that sources of mechanical energy

(i.e. active star formation) may be of central importance (see Guillemin & Bergeron 1997). Extended multiphase halos are seen preferentially around late-type spiral galaxies with signs of elevated star formation (see Dahlem 1998 and references therein). In fact, a basic scenario which might explain both the taxonomy of Mg II absorbers (especially the Double and CIV-deficient systems) and the CIV-Mg II kinematics connection, is one in which star formation processes accelerate hot, ionized gas outward, which subsequently cools and fragments into parcels of low ionization gas (e.g. Houck & Bregman 1990; Li & Ikeuchi 1992; Avillez 1999). These parcels would be observed as outlying kinematic components in the Mg II profiles.

These points are somewhat suggestive of a causal connection between evolution in the cosmic star formation rate and absorbing gas cross sections, kinematics, and ionization conditions. If true, we could hypothesize that scenarios of a cosmic mean history of galaxy evolution inferred from the global record of star formation history should be fully consistent with one based upon an “absorption line perspective”.

The global star formation rate appears to drop below $z \sim 1.0$ (Lilly et al. 1996; Madau, Lucia, & Dickinson 1998; however, see Cowie, Songaila, & Barger 1999), implying a reduction in the (infalling) gas reservoir for galaxies. It could be that a majority of galaxies transform into self-regulatory systems by $z \sim 1$ and begin to evolve in a more isolated fashion and in a direction dependent upon their ability to continue forming stars. Galaxies that are rich in gas and capable of forming large numbers of molecular clouds in their interstellar media (i.e. late-type galaxies) would continue to form stars and exhibit evolution, whereas those less capable would exhibit no

discernable evolution. Such a scenario is consistent with the differential luminosity evolution reported by Lilly et al. (1995) and is not inconsistent with the tentative trends we see between galaxy color and ionization conditions (also see Guillemin & Bergeron 1997).

It is unfortunate that there currently are no Mg II absorption-line samples for the highest redshifts ($z > 2.2$), so an absorption line perspective cannot yet be fully appreciated [however, see the theoretical predictions of Rauch, Haehnelt, & Steinmetz (1997)].

Support for this work was provided by the NSF (AST-9617185), and NASA (NAG 5-6399 and AR-07983.01-96A) the latter from the Space Telescope Science Institute, which is operated by AURA, Inc., under NASA contract NAS5-26555. R. R. M. was supported by an NSF REU supplement. B. T. J. acknowledges support from NOAO, which is operated by AURA, Inc., under cooperative agreement with the NSF. We thank Eric Feigelson for several very informative discussions on the statistical treatment of data and as a valuable resource of additional information. Sandhya Rao and David Turnshek kindly shared unpublished data of Mg II/DLA-selected galaxy properties, for which we are grateful. We thank David Bowen for providing CIV data prior to their publication and for an electronic version of the Mg II $\lambda 2796$ profile from the GHRS spectrum of SN 1993J. We also thank Bill Matthews for an enlightening discussion on the properties of gas and star formation in elliptical galaxies and the anonymous referee for a careful reading of the manuscript that lead to significant improvements.

REFERENCES

- Avillez, M. A., 1999, in *The Stromlo Workshop on High Velocity Clouds*, ASP Conference Series, Vol. 666, in press (astro-ph/9901056)
- Babu, G. J., & Feigelson, E. D. 1996, *Astrostatistics*, (London : Chapman & Hall)
- Bahcall, J. N., et al. 1993, *ApJS*, 87, 1
- Bahcall, J. N., et al. 1996, *ApJ*, 457, 19
- Bechtold, J., Green, R. F., & York, D. G. 1987, *ApJ*, 312, 50
- Bergeron, J., & Boissé, P. 1984, *A&A*, 133, 374
- Bergeron, J., & Boissé, P. 1991, *A&A*, 243, 344
- Bergeron, J., Christiani, S., & Shaver, P. 1992, *A&A*, 257, 417
- Bergeron, J., et al. 1994, *ApJ*, 436, 33
- Boissé, P., & Bergeron, J. 1985, *A&A*, 145, 59
- Boissé, P., Le Brun, V., Bergeron, J., Deharveng, J.-M. 1998, *A&A*, 333, 841
- Bowen, D. V., 1999, private communication
- Bowen, D. V., & Blades, J. C. 1993, *ApJ*, 403, 55
- Bowen, D. V., Blades, J. C., & Pettini, M. 1996, *ApJ*, 472, L77
- Bowen, D. V., Blades, J. C., & Pettini, M. 1995, *ApJ*, 448, 634
- Bruzual, G., & Charlot, S. 1993, *ApJ*, 405, 538
- Carilli, C. L. & van Gorkom, J. H. 1992, *ApJ* 399, 373
- Charlton, J. C., & Churchill, C. W. 1996, *ApJ*, 465, 631
- Charlton, J. C., & Churchill, C. W. 1998, *ApJ*, 499, 181
- Churchill, C. W. 1997, Ph.D. Thesis, University of California, Santa Cruz
- Churchill, C. W., & Charlton, J. C. 1999, *AJ*, 118, 59
- Churchill, C. W., Rigby, J. R., Charlton, J. C., & Vogt, S. S. 1999a, *ApJS*, 120, 51
- Churchill, C. W., Mellon, R. R., Charlton, J. C., Jannuzi, B. T., Kirhakos, S., Steidel, C. C., & Schneider, D. P. 1999b, *ApJ*, 519, L43
- Churchill, C. W., Mellon, R. R., Charlton, J. C., Jannuzi, B. T., Kirhakos, S., Steidel, C. C., & Schneider, D. P. 2000, *ApJ*, submitted (Paper I)
- Churchill, C. W., Steidel, C. C., & Vogt, S. S. 1996, *ApJ*, 471, 164
- Cowie, L. L., Songaila, A., & Barger, A. J. 1999, *AJ*, 118, 603
- Dahlem, M. 1998, *PASP*, 109, 1298
- Ferland, G. J. 1996, *Hazy*, University of Kentucky Internal Report
- Guillemin, P., & Bergeron, J. 1997, *A&A*, 328, 499
- Haardt, F., & Madau, P. 1996, *ApJ*, 461, 20
- Hernquist, L., & Mihos, J. C., *ApJ*, 488, 41
- Houck, J. C., & Bregman, J. N. 1990, *ApJ*, 352, 506
- Hibbard, J. E., & van Gorkom, J. H. 1996, *AJ*, 111, 655
- Hubble, E. 1936, *The Realm of the Nebulae*, (New Haven : Yale University Press)
- Hummel, E., van der Hulst, J. M., Kennicutt, R. C., & Keel, W. C. 1990, *A&A*, 236, 333
- Irwin, J. I. 1995, *PASP*, 107, 715
- Jannuzi, B. T., et al. 1998, *ApJS*, 118, 1
- Johnson, R. A., & Wichern, D. W. 1992, *Applied Multivariate Statistical Analysis*, (Upper Saddle River : Prentice-Hall)
- Knapp, G. R., Turner, E. L., & Cunniffe, P. E. 1985, *AJ*, 90, 454
- Lanzetta, K. M., & Bowen, D. V. 1992, *ApJ*, 357, 321
- Lanzetta, K. M., & Bowen, D. V. 1992, *ApJ*, 391, 48
- Lanzetta, K. M., Turnshek, D. A., & Wolfe, A. M. 1987, *ApJ*, 322, 739
- La Valley, M., Isobe, T., & Feigelson, E. 1992, in *Astronomical Data Analysis Software and Systems I*, ASP Conf. Series, V25, D.M. Worrall, C. Biemesderfer, & J. Barnes, eds., 245
- Le Brun, V., Bergeron, J., Boissé, P., & Christian, C. 1993, *A&A*, 297, 33
- Le Brun, V., Bergeron, J., Boissé, P., & Deharveng, J. M. 1997, *A&A*, 321, 733
- Le Fèvre, O., Abraham, R., Lilly, S. J., Ellis, R. S., Brinchmann, J., Schade, D., Tresse, L., Colles, M., Crampton, D., Glazebrook, K., Hammer, F., & Broadhurst, T. 1999, *MNRAS*, in press (astro-ph/990921)
- Li, F., & Ikeuchi, S. 1992, *ApJ*, 390, 405
- Lilly, S. J., Le Fèvre, O., Hammer, F., & Crampton, D. 1996, *ApJ*, 460, L1
- Lilly, S. J., Tresse, L., Hammer, F., Crampton, D., Le Fèvre, O. 1995, *ApJ*, 455, 108
- Lu, L., Sargent, W. L. W., Barlow, T. A., Churchill, C. W., & Vogt, S. S. 1996, *ApJS*, 107, 475
- Lutz, D. 1992, *A&A*, 315, L137
- Madau, P., Lucia, P. & Dickinson, M. 1998, *ApJ*, 498, 106
- Mathews, W. G., & Brighenti, F. 1998, in *Galactic Halos: A UC Santa Cruz Workshop*, ASP Conf. Series, V136, ed. D. Zaritsky (San Francisco : PASP), 277
- McLin, K. M., Giroux, M. L., & Stocke, J. T. 1998, in *Galactic Halos: A UC Santa Cruz Workshop*, ASP Conf. Series, V136, ed. D. Zaritsky (San Francisco : PASP), 175
- Mo, H. J., & Miralda-Escudé, J. 1996, *ApJ*, 469, 589
- More, J. J. 1978, in *Numerical Analysis Proceedings*, ed. G.A. Watson, *Lecture Notes in Mathematics* (Garching : Springer-Verlag), 630
- Morganti, R., Oosterloo, T., & Tsvetanov, Z. 1998, *AJ*, 115, 915
- Mukherjee, S., Feigelson, E. D., Babu, G. J., Murtagh, F., Fraley, C., & Raftery, A. 1998, *ApJ*, 508
- Mulchaey, J. S., Mushotzky, R. F., Burstein, D., & Davis, D. S. 1996, *ApJ*, 456, L5

- Neuschaefer, L. W., Im, M., Ratnatunga, K. U., Griffiths, R. E., & Casertano, S. 1997, *ApJ*, 480, 59
- O'Connell, R. W. 1999, *ARA&A*, in press (astro-ph/9906068)
- Patton, D. R., Pritchett, C. J., Yee, H. K. C., Ellingson, E., & Carlberg, R. G. 1997, *AJ*, 475, 29
- Petitjean, P., & Bergeron, J. 1990, *A&A*, 231, 309
- Petitjean, P., & Bergeron, J. 1994, *A&A*, 283, 759
- Pettini, M., Steidel, C. C., Adelberger, K. L., Dickinson, M., & Giavalisco, M. 1999, *ApJ*, in press (astro-ph/9908007)
- Rao, S. M., & Turnshek, D. A. 1998, *ApJ*, 500, L115
- Rao, S. M., & Turnshek, D. A. 1999, (astro-ph/9909164)
- Rauch, M., Haehnelt, M. G., & Steinmetz, M. 1997, *ApJ*, 481, 601
- Rigby, J. R., Charlton, J. C., Churchill, C. W., Jannuzi, B. T., Kirhakos, S., & Vogt, S. S. 1999, in preparation
- Sargent, W. L. W., Boksenberg, A., & Steidel, C. C., 1988, *ApJS*, 68, 539
- Savage, B. D., & Sembach, K. R. 1991, *ApJ*, 379, 245
- Savage, B. D., Sembach, K. R., & Lu, L. 1997, *AJ*, 113, 2158
- Sembach, K. R., & Savage, B. D. 1992, *ApJS*, 83, 147
- Sembach, K. R., Savage, B. D., & Hurwitz, M. 1999, astro-ph/9905343
- Steidel, C. C. 1993, in *The Environment and Evolution of Galaxies*, eds. J. M. Shull & H. A. Thronson, Jr. (Dordrecht : Kluwer), 263
- Steidel, C. C. 1995, in *QSO Absorption Lines*, ed. G. Meylan (Garching : Springer Verlag), 139
- Steidel, C. C. 1998, in *Galactic Halos: A UC Santa Cruz Workshop*, ASP Conf. Series, V136, ed. D. Zaritsky (San Francisco : PASP), 167
- Steidel, C. C., Dickinson, M., Meyer, D. M., Adelberger, K. L., & Sembach, K. R. 1997, *ApJ*, 480, 568
- Steidel, C. C., Dickinson, M., & Persson, E. 1994, *ApJ*, 437, L75
- Steidel, C. C., & Sargent, W. L. W. 1992, *ApJS*, 80, 1
- van Gorkom, J. H. 1992, in *Morphological and Physical Classifications of Galaxies*, eds. G. Longo, M. Capaccioli, & G. Busarello (Kluwer Academic), 223
- Vogt, S. S., et al. 1994, in *Proceedings of the SPIE*, 2128, 326
- Ward, J. H. 1963, *Journal of the American Statistical Association*, 58, 236
- Yanny, B. 1992, *PASP*, 104, 840
- Yanny, B., and York, D. G. 1992, *ApJ*, 391, 569

TABLE 1
ABSORBER PROPERTIES

QSO	z_{abs}	$W(\text{MgII})$ [Å]	ω_v [km/s]	N_{cl}	$W(\text{FeII})$ [Å]	$W(\text{CIV})$ [Å]	$W(\text{Ly}\alpha)$ [Å]	Samples ^c	Class
0002 + 051	0.5915	0.103 ± 0.008	5.0 ± 0.7	1	< 0.012	< 0.23 ^a	...	IC	Sngl/Wk
	0.8514	1.086 ± 0.016	97.1 ± 4.6	12	0.419 ± 0.022	1.26 ± 0.06	2.47 ± 0.08	CA	Double
	0.8665	0.023 ± 0.008	1.7 ± 0.5	1	< 0.010	< 0.11 ^a	0.81 ± 0.10	IC	Sngl/Wk
	0.9560	0.052 ± 0.007	6.2 ± 1.0	1	< 0.005	0.52 ± 0.04	0.85 ± 0.07	CA,IC	Sngl/Wk
0058 + 019	0.6127	1.625 ± 0.013	50.8 ± 0.3	7	1.274 ± 0.037	...	6.77 ± 0.40		DLA/HI
	0.7252	0.253 ± 0.012	9.3 ± 0.5	1	< 0.034	...	0.46 ± 0.13		Sngl/Wk
0117 + 213	0.5764	0.906 ± 0.100	26.9 ± 1.0	4	0.270 ± 0.050 ^a	0.58 ± 0.06	11.15 ± 1.09	CA	DLA/HI
	0.7291 ^b	0.238 ± 0.009	44.2 ± 0.9	5	0.075 ± 0.016	< 0.10	...	IC	CIV-def
	1.0480	0.415 ± 0.009	39.1 ± 0.7	7	0.065 ± 0.010	< 0.08	1.93 ± 0.04	CA,IC	CIV-def
	1.3250	0.291 ± 0.011	76.1 ± 1.5	6	0.026 ± 0.009	0.89 ± 0.03	1.51 ± 0.03	CA,IC	Classic
	1.3430 ^b	0.153 ± 0.008 ^a	34.8 ± 2.9	5	0.029 ± 0.004 ^a	0.67 ± 0.02	1.19 ± 0.04	CA,IC	Classic
0454 - 220	0.4744	1.382 ± 0.009	40.8 ± 1.0	8	0.975 ± 0.029	0.63 ± 0.03	3.74 ± 0.05	CA	DLA/HI
	0.4833	0.431 ± 0.007	15.5 ± 0.5	7	0.162 ± 0.043	0.38 ± 0.11	1.56 ± 0.03	CA,IC	CIV-def
0454 + 039	0.6428	0.118 ± 0.008	4.8 ± 0.6	1	0.037 ± 0.014	0.38 ± 0.03	0.70 ± 0.05	CA,IC	Sngl/Wk
	0.8596	1.445 ± 0.014	42.8 ± 1.3	12	1.232 ± 0.014	0.59 ± 0.04	10.70 ± 0.26	CA	DLA/HI
	0.9315	0.042 ± 0.005	4.4 ± 0.9	1	0.030 ± 0.008 ^a	< 0.62	0.31 ± 0.07	IC	Sngl/Wk
0823 - 223	1.1532 ^b	0.432 ± 0.012	24.1 ± 1.7	7	0.084 ± 0.015	0.94 ± 0.06	1.56 ± 0.01	CA,IC	Classic
	0.7055	0.092 ± 0.007	11.9 ± 0.7	1	< 0.008	< 0.18	...	IC	Sngl/Wk
	0.9110 ^b	1.276 ± 0.016	87.1 ± 1.1	18	0.416 ± 0.026	1.34 ± 0.06	2.68 ± 0.07	CA,IC	Double
0958 + 551	1.2113	0.060 ± 0.007	3.4 ± 1.1	1	< 0.006	...	< 0.92		Sngl/Wk
	1.2724	0.081 ± 0.007	4.9 ± 0.6	1	0.017 ± 0.004	0.44 ± 0.03	0.75 ± 0.15	CA,IC	Sngl/Wk
1206 + 459	0.9276	0.878 ± 0.016	116.2 ± 4.8	12	0.077 ± 0.020	1.84 ± 0.52	2.47 ± 0.07	CA,IC	Double
	0.9343	0.049 ± 0.005	7.7 ± 0.8	1	< 0.004	0.25 ± 0.05	0.47 ± 0.07	CA,IC	Sngl/Wk
1241 + 176	0.5505	0.481 ± 0.019	33.9 ± 4.1	4	0.236 ± 0.048	0.83 ± 0.07	...	IC	Classic
	0.5584	0.135 ± 0.014	17.2 ± 1.1	4	< 0.012	0.21 ± 0.06	...	IC	Sngl/Wk
	0.8955	0.018 ± 0.005	5.0 ± 1.2	1	< 0.005	< 0.10	0.45 ± 0.05	IC	Sngl/Wk
1248 + 401	0.7730	0.694 ± 0.009	53.6 ± 2.6	8	0.247 ± 0.020	0.65 ± 0.06	1.45 ± 0.04	CA,IC	Classic
	0.8546 ^b	0.235 ± 0.014	39.4 ± 3.9	7	0.031 ± 0.007	0.68 ± 0.06	1.46 ± 0.29	CA,IC	Classic
1317 + 277	0.6601 ^b	0.338 ± 0.011	36.1 ± 2.2	8	0.126 ± 0.016	< 0.14	1.48 ± 0.03	CA,IC	CIV-def
1329 + 412	0.5008	0.258 ± 0.035	25.6 ± 1.4	4	< 0.100	< 0.40	...	A	CIV-def
	0.8933	0.400 ± 0.023	55.0 ± 2.8	4	0.080 ± 0.035	< 0.12 ^a	1.15 ± 0.16	A,CA	CIV-def
	0.9739	0.181 ± 0.035	26.8 ± 2.7	4	< 0.028	0.87 ± 0.05	1.15 ± 0.23	CA	Classic
	0.9984	0.142 ± 0.010	6.7 ± 0.7	1	0.058 ± 0.017	< 0.11	0.31 ± 0.20	CA	Sngl/Wk
	1354 + 195	0.4566	0.751 ± 0.023	31.9 ± 1.7	7	0.149 ± 0.088	0.91 ± 0.04	1.72 ± 0.08	CA
1622 + 238	0.5215	0.030 ± 0.007	6.6 ± 1.1	1	< 0.012	< 0.24	1.08 ± 0.08	IC	Sngl/Wk
	0.4720	0.681 ± 0.048	25.6 ± 3.1	1	< 0.118	0.46 ± 0.14	1.27 ± 0.27	A	Classic:
	0.6561	1.449 ± 0.029	44.7 ± 2.3	3	1.015 ± 0.050	0.29 ± 0.09	9.42 ± 0.34	A,CA	DLA/HI
1634 + 706	0.7971	0.274 ± 0.029	45.2 ± 2.8	4	< 0.092	1.25 ± 0.06	1.38 ± 0.14	CA	Classic
	0.8913	1.534 ± 0.025	50.7 ± 2.0	10	1.080 ± 0.421	0.82 ± 0.05	2.98 ± 0.10	CA	DLA/HI
	0.8182	0.030 ± 0.018	3.1 ± 1.6	1	< 0.008	< 0.07	...	IC	Sngl/Wk
	0.9056	0.064 ± 0.004	4.1 ± 0.6	1	< 0.005	0.18 ± 0.02	0.49 ± 0.03	CA,IC	Sngl/Wk
	0.9902	0.558 ± 0.005	17.8 ± 0.2	5	0.127 ± 0.011	0.32 ± 0.02	1.09 ± 0.03	CA,IC	CIV-def
2128 - 123	1.0414	0.097 ± 0.008	17.2 ± 1.1	4	< 0.038	0.40 ± 0.02	1.42 ± 0.01	CA,IC	Sngl/Wk
2145 + 067	0.4297	0.406 ± 0.014	15.8 ± 0.4	4	< 0.260 ^a	0.40 ± 0.04	2.92 ± 0.08	CA	CIV-def
	0.7908	0.483 ± 0.015	75.1 ± 1.1	6	0.041 ± 0.014	1.13 ± 0.08	1.22 ± 0.04	CA,IC	Classic

^a Not “flag” transition; see system notes (§3)

^b Measurement of ω_v was censored (see text). Uncensored values are 46.8 km s⁻¹ (0117 + 213, $z = 0.7291$), 45.1 km s⁻¹ (0117 + 213, $z = 1.3430$),

^c Sample A: systems with $W(\text{MgII})$ detection limits greater than 0.3 Å. Sample CA: systems used for multivariate Cluster Analysis

Sample IC: systems used for Ionization Conditions analysis.

TABLE 2
GALAXY PROPERTIES

QSO	z_{abs}	M_B	M_K	$B - K$	$D h^{-1}$ (kpc)	Reference
0002 + 051	0.5915	-21.1	-25.2	4.1	23.8	Churchill et al. (1996)
	0.8514	-21.2	-24.1	2.9	18.6	Churchill et al. (1996)
0058 + 051	0.6127 ^a	-19.6	-22.7	3.1	19.3	This paper
0117 + 213	0.5764	-21.9	-25.9	4.0	5.1	Churchill et al. (1996)
	0.7291	-22.3	-26.3	4.0	36.0	Churchill et al. (1996)
0454 + 039	0.8596	-19.5	> -23.4	< 3.9	10.6	Churchill et al. (1996)
	1.1532 ^b	-21.0	-23.8	2.8	40.1	This paper
1241 + 176	0.5505	-20.5	-23.9	3.4	13.8	Churchill et al. (1996)
1248 + 401	0.7730	-20.3	-23.5	3.2	23.3	Churchill et al. (1996)
1317 + 277	0.6601	-21.9	-25.7	3.8	37.6	Churchill et al. (1996)
1354 + 195	0.4566	-20.7	-23.8	3.0	26.2	This paper
1622 + 238	0.4720	-19.5	-22.2	2.7	22.2	Steidel et al. (1997)
	0.7971	-21.5	-24.6	3.0	46.5	Churchill et al. (1996), Steidel et al. (1997)
	0.8913	-20.6	-23.7	3.1	15.0	Churchill et al. (1996), Steidel et al. (1997)
2128 - 123	0.4297	-21.4	-24.7	3.3	31.6	This paper
2145 + 067	0.7908	-21.6	-24.5	3.0	29.3	This paper

^a Recent analysis of a WFPC2/*HST* image revealed a previously unseen galaxy within 1'' of the QSO. This galaxy identification should be viewed with caution.

^b M_B extrapolated from \mathfrak{R} -band image using an Im spectroscopic template consistent with the $R - K$ color.

TABLE 3
MgII AND CIV EQUIVALENT WIDTHS^a FROM THE LITERATURE

QSO	z_{abs}	$W(\text{MgII}) [\text{\AA}]$	$W(\text{CIV}) [\text{\AA}]$	References
Mrk 205	0.004	0.29	0.19	BB93
1219 + 047	0.005	1.96	1.28	BBP96
0955 + 326	0.005	2.56	0.85	B99,J98
1543 + 489	0.075	0.61	< 0.26	BBP95
1137 + 660	0.1164	0.50	< 0.32	B94
1704 + 608	0.2216	0.45	0.43	B94
1317 + 277	0.2891	0.33	0.45	B94
1634 + 706	0.6694	0.29	< 0.07	B94
0454 + 034	1.1535	0.57	0.95	SS92
1101 - 264	1.1875	0.41	0.97	BB85
1101 - 264	1.2030	0.59	0.57	BB85
1247 + 265	1.2233	0.48	0.67	SS92
1602 - 002	1.3245	0.64	< 0.43	LTW87
0226 - 035	1.3277	0.83	0.43	SS92
1421 + 122	1.3605	0.43	0.34	LTW87
0237 - 232	1.3647	2.05	1.52	SS92
0957 + 561	1.3901	2.10	0.27	BB84
0058 + 016	1.4641	0.45	0.40	SS92
0002 - 422	1.5413	0.48	0.71	LTW87
0424 - 131	1.5615	0.38	1.05	SS92
1329 + 412	1.6012	0.70	1.38	SS92
1017 + 276	1.6081	0.11	0.37	SS92
0237 - 232	1.6363	0.78	0.08	SS92
0421 + 016	1.6375	0.35	1.13	SS92
1246 - 054	1.6466	0.52	0.79	SS92
0237 - 232	1.6583	0.76	1.14	SS92
0237 - 232	1.6732	1.31	1.63	SS92
1311 - 270	1.6860	0.83	< 0.38	LTW87
0958 + 551	1.7320	0.37	1.01	SS92
0854 + 191 ^b	1.7342	4.14	1.14	SS92
1017 + 276	1.7953	2.04	1.51	SS92
1331 + 170	1.7860	1.05	0.17	SS92
1331 + 170	1.7766	1.33	1.63	SS92
0100 + 130	1.7971	1.11	0.93	SS92
1704 + 710	1.8107	0.58	0.54	SS92
1329 + 412	1.8355	0.49	0.13	SS92
1101 - 264	1.8386	1.00	0.31	LTW87
1228 + 077	1.8966	1.72	0.90	LTW87
1435 + 635	1.9235	1.05	0.46	SS92
0551 - 366 ^b	1.9613	5.80	2.13	LTW87
0119 - 044	1.9638	0.52	1.68	SS92
0013 - 003 ^b	1.9713	7.37	2.19	SS92
2126 - 158	2.0219	0.67	0.99	LTW87
0013 - 003 ^b	2.0290	5.75	0.63	SS92
0348 + 061	2.0237	0.59	0.82	SS92
0424 - 131	2.0344	1.10	< 0.12	SS92
0450 - 131	2.0667	2.20	1.07	SS92

^a Equivalent widths are rest frame.

^b Does not appear on Figure 14.

References:— (BB84) Bergeron & Boissé 1984; (BB85) Boissé & Bergeron 1985; (LTW87) Lanzetta et al. 1987; (BB93) Bowen & Blades 1993; (B94) Bergeron et al. 1994; (BBP95) Bowen et al. 1995; (BBP96) Bowen et al. 1996; (SS92) Steidel & Sargent 1992; (J98) Jannuzi et al. 1998; (B99) Bowen 1999.

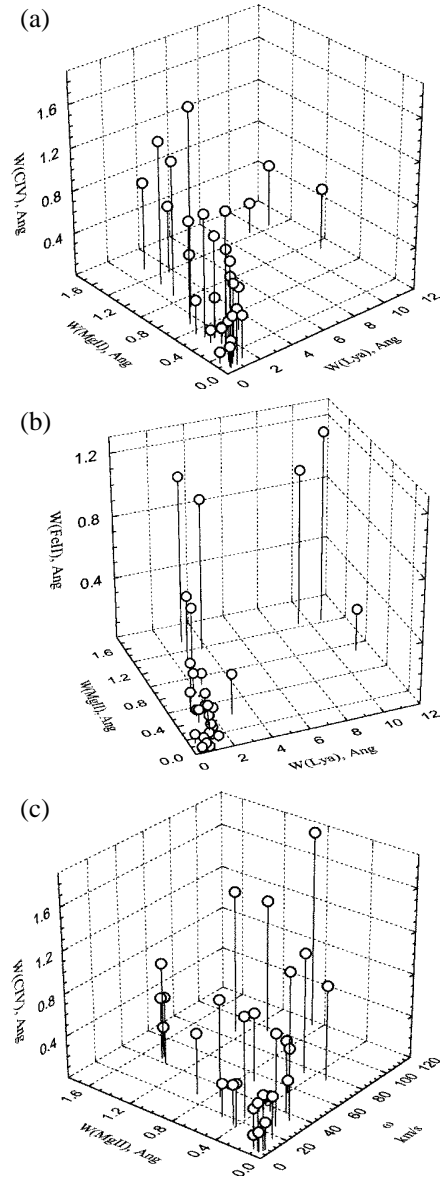


FIG. 1.— Three dimensional scatter plots of (a) $W_r(\text{MgII})$ vs. $W_r(\text{Ly}\alpha)$ vs. $W_r(\text{CIV})$, (b) $W_r(\text{MgII})$ vs. $W_r(\text{Ly}\alpha)$ vs. $W_r(\text{FeII})$, (c) $W_r(\text{MgII})$ vs. ω_v vs. $W_r(\text{CIV})$. Upper limits on FeII and CIV, of which a few are present near the origin, are plotted but not delineated. Vertical lines intersect the x - y values (right handed coordinate system) in the x - y plane. The z value of a datum can be obtained by projecting a line from the point to the background mesh in a direction parallel to the constant z lines in the mesh.

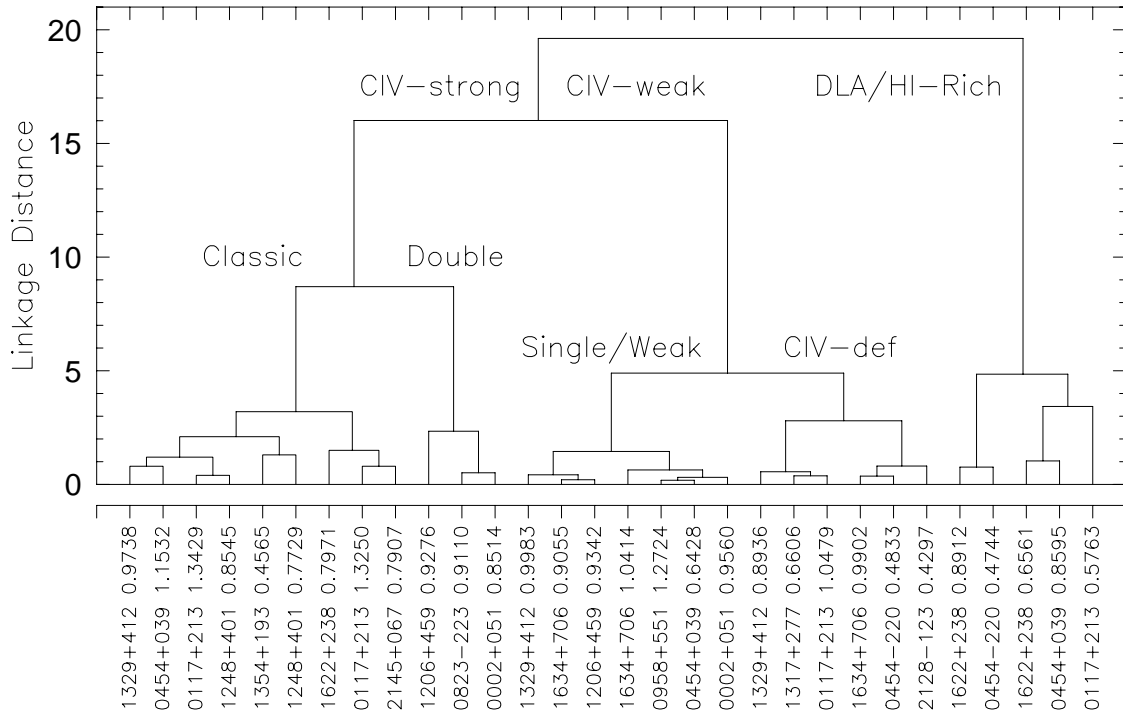


FIG. 2.— Tree cluster diagram showing linkage distance in a subsample of 30 absorbers, with each labeled across the bottom. The discriminating absorption properties are $W_r(\text{MgII})$, $W_r(\text{Ly}\alpha)$, $W_r(\text{CIV})$, $W_r(\text{FeII})$, and ω_v , using a $N(0, 1)$ standardization (see text). A Ward's amalgamation algorithm was used with Euclidean distance. The isolated branches with linkages greater than ~ 4 are given classifications based upon the cluster means (see Figure 3).

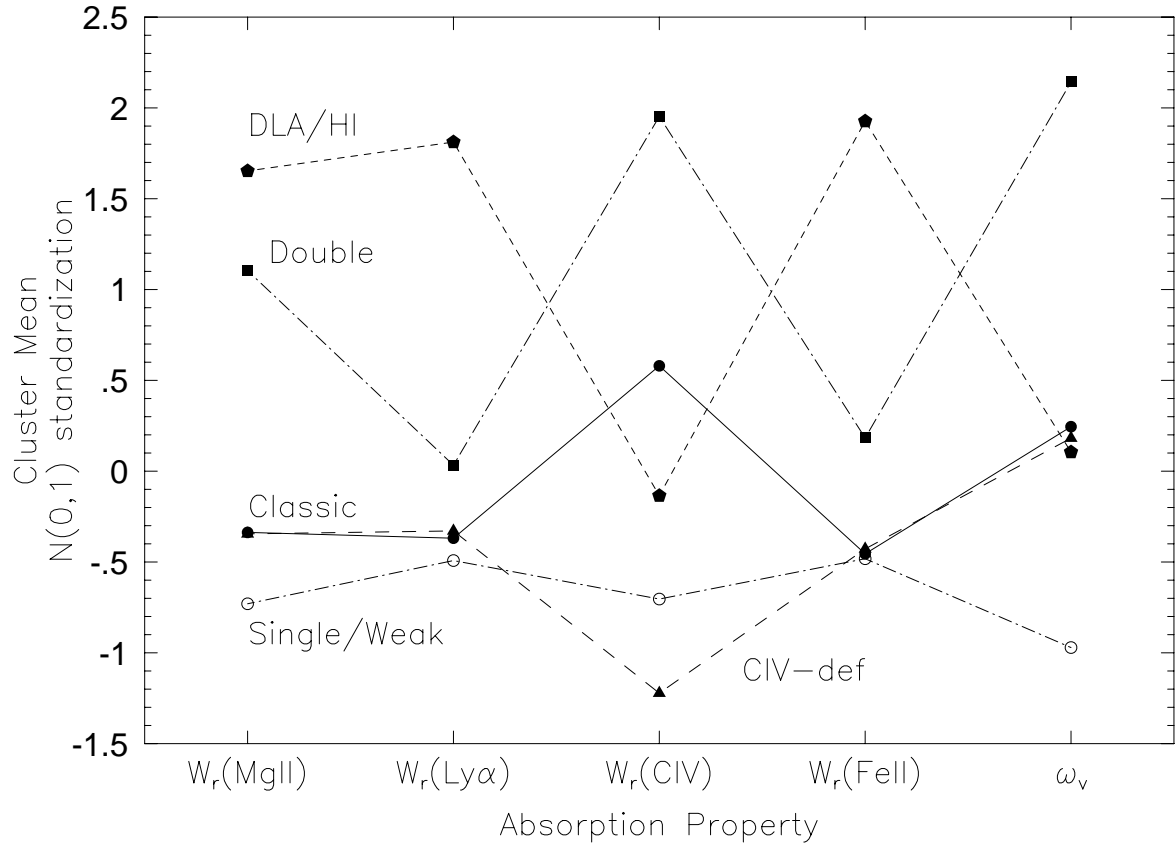


FIG. 3.— K -means cluster diagram for $K = 5$ showing the mean values $W_r(\text{MgII})$, $W_r(\text{Ly}\alpha)$, $W_r(\text{CIV})$, $W_r(\text{FeII})$, and ω_v , placed on a $N(0, 1)$ standardization (see text), for *each* of the five clusters shown in Figure 2. With this standardization, zero is the mean value and ± 1 is the standard deviation for a given absorption property. The cluster classifications are given on the left hand side.

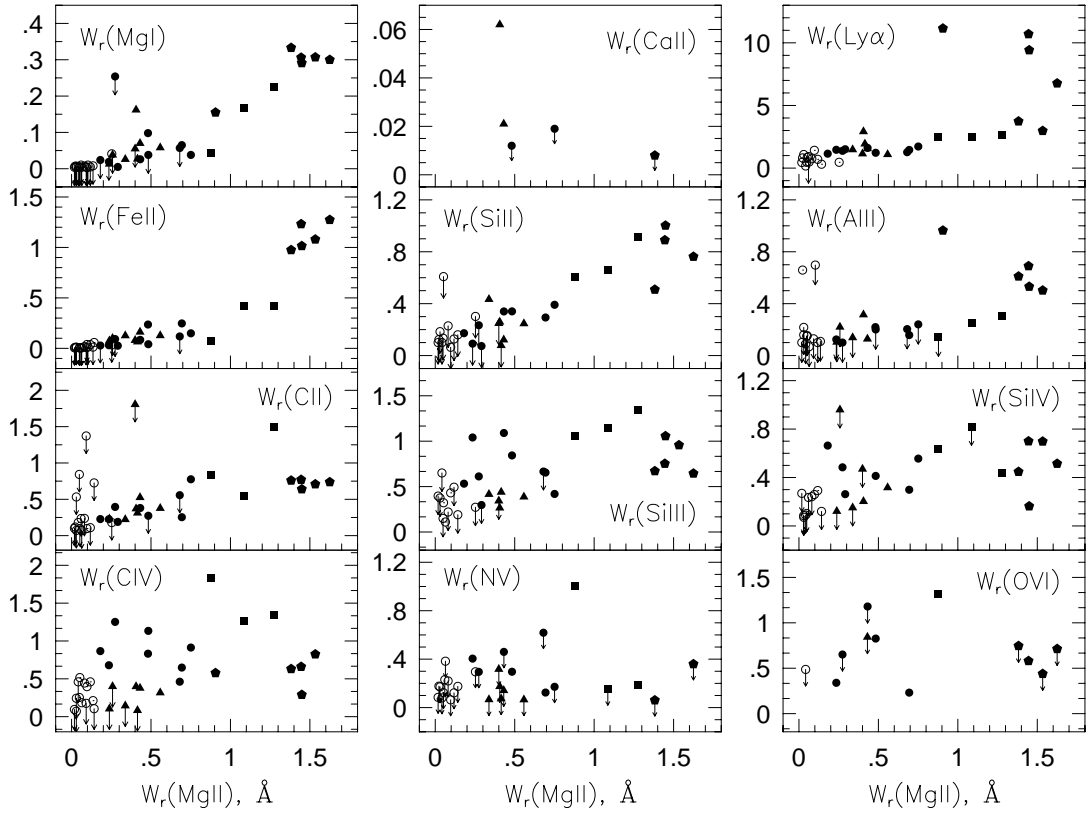


FIG. 4.— The rest-frame equivalent widths of the elemental species listed in Table 1 and in Tables 3 and 4 from Paper I vs. that of MgII $\lambda 2796$. Also included is CaII. The panels are in order of increasing ionization potential from the upper left to the lower right. Data point types denote the various absorber classes, and are the same as in Figure 3. Downward pointing arrows denote upper limits.

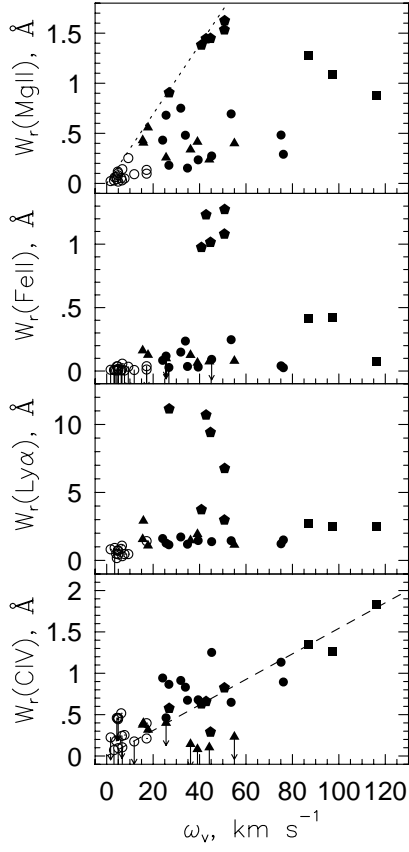


FIG. 5.— The rest-frame equivalent widths of Mg II, Fe II, Ly α , and CIV vs. the Mg II kinematic spread, ω_v . Data point types denote the various absorber classes, and are the same as in Figure 3.

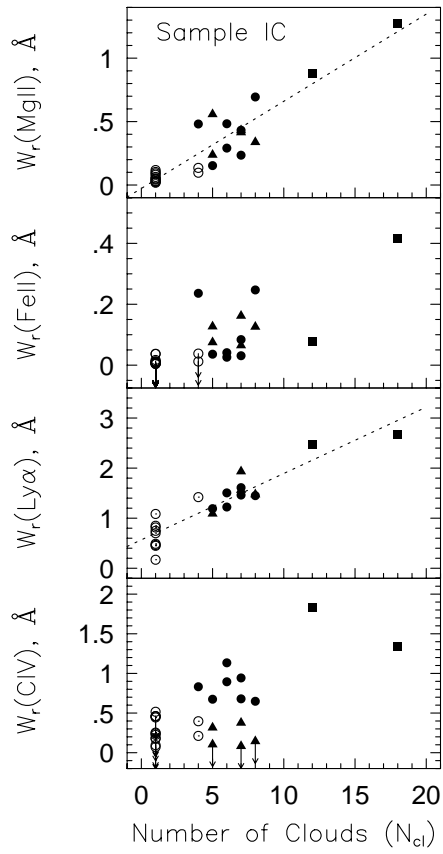


FIG. 6.— The rest-frame equivalent widths of Mg II, Fe II, Ly α , and CIV vs. the number of Voigt profile components, or clouds, N_{cl} . Only Sample IC is presented for reasons given in the text. Data point types denote the various absorber classes, and are the same as in Figure 3.

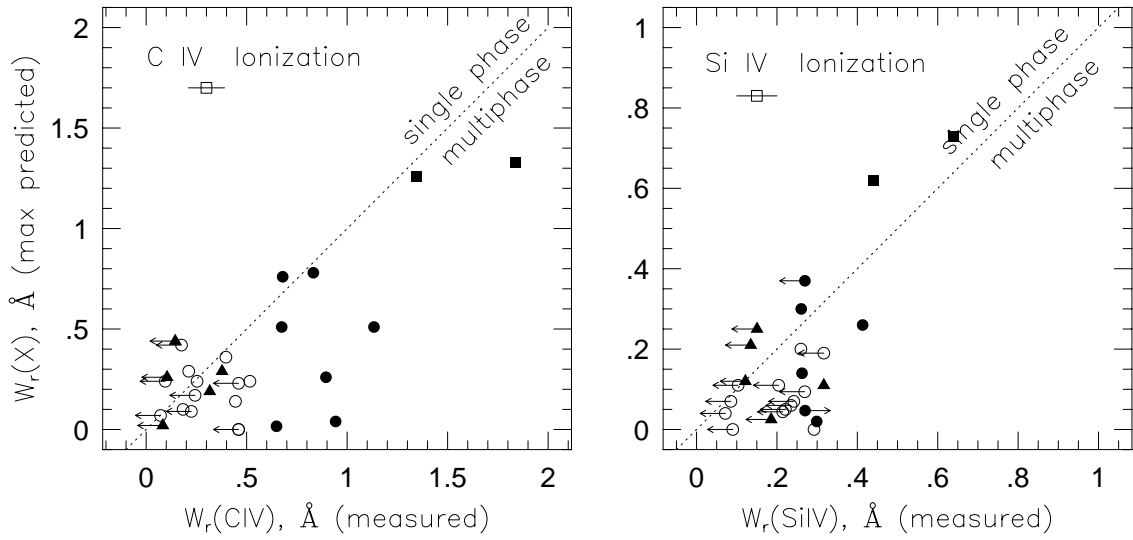


FIG. 7.— The *maximum* $W_r(\text{CIV})$ (left panel) and $W_r(\text{SiIV})$, under the assumption of extremely high photoionization equilibrium, that can arise in single phase MgII clouds vs. the measured rest-frame equivalent widths. The predicted points are based upon CLOUDY models of the systems (Sample IC), incorporating the number of clouds and their column densities, b parameters, and kinematics (see text for details). If a system lies below the line, then the measured CIV or SiIV cannot arise solely in the MgII clouds, but must arise in a distinct highly ionized phase that does not give rise to detectable amounts of MgII. The typical error bar of the measure data are given in the upper left corners of both panels. Data point types denote the various absorber classes.

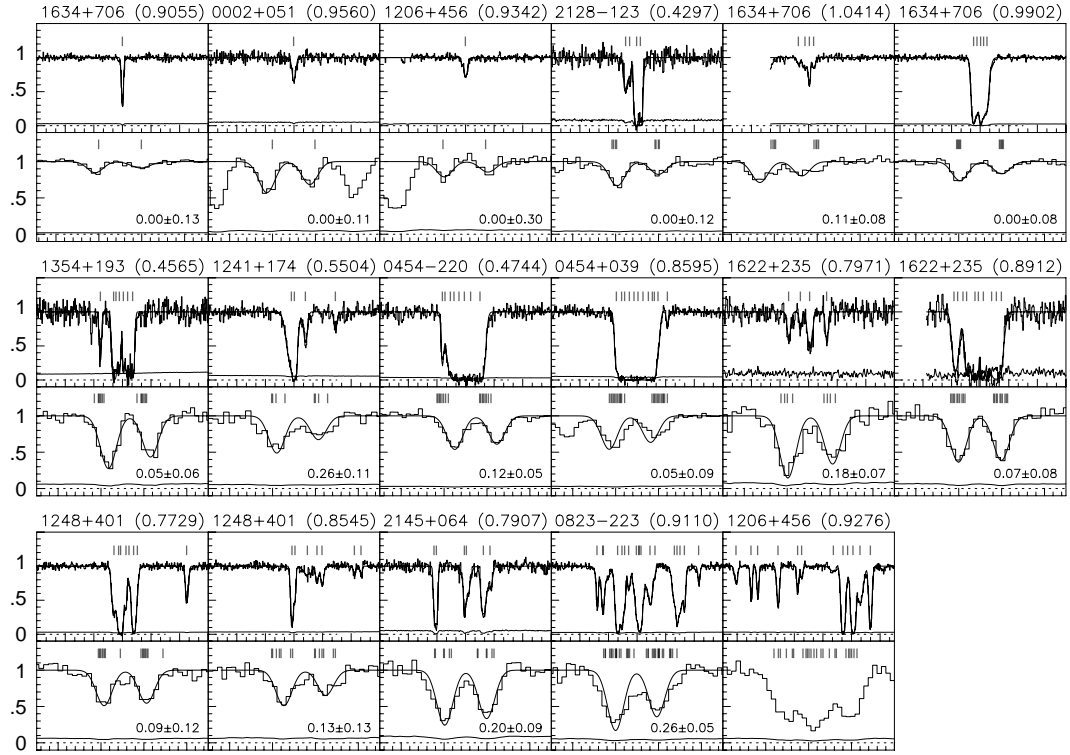


FIG. 8.— The CIV kinematics. Shown are the MgII $\lambda 2796$ transitions and CIV $\lambda\lambda 1548, 1550$ doublets of the 17 systems for which both members of the CIV doublet are detected and unblended with other transitions in the FOS spectra. The panels with MgII show a velocity window of 600 km s^{-1} , centered on the system zero point. Ticks above the continuum give the Voigt profile component velocities and the smooth curves through the data are the Voigt profile fit results. The panels with the CIV doublets show a velocity window of 2000 km s^{-1} . The MgII Voigt profile velocities are projected over the continuum of each doublet. The smooth curves through the data are single Gaussian fits with the widths held at the instrumental resolution, but with the centroids and depths allowed to vary.

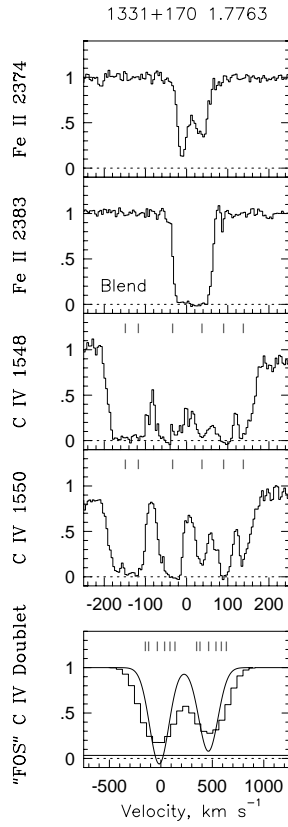


FIG. 9.— The Fe II and C IV kinematics of a DLA at $z = 1.7763$ toward Q 1331 + 170; the Mg II profiles were not covered due to the setting of the HIRES echelle. The upper panels show HIRES/Keck data at $R = 22,500$ over a velocity window of 500 km s^{-1} . Ticks above the C IV roughly give the kinematic composition of the high ionization gas. The lower panel shows simulated FOS spectra of the C IV doublet over a velocity window of 2000 km s^{-1} . As with Figure 8, single Gaussian fits with widths held at the instrumental resolution are superimposed on the data.

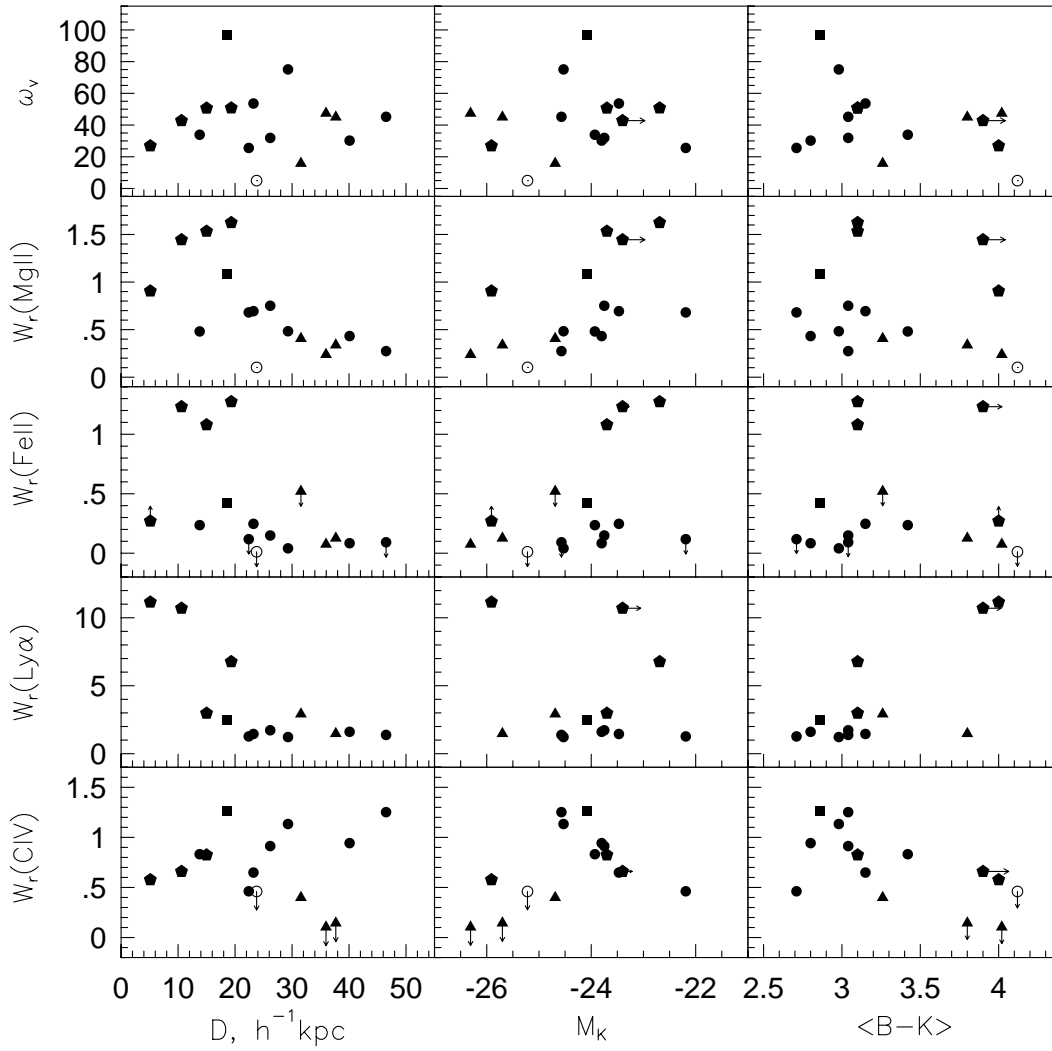


FIG. 10.— The Mg II kinematic spread, and Mg II, Fe II, Ly α , and C IV absorption strengths vs. host galaxy impact parameter, absolute K magnitude, and rest-frame $B - K$ color.

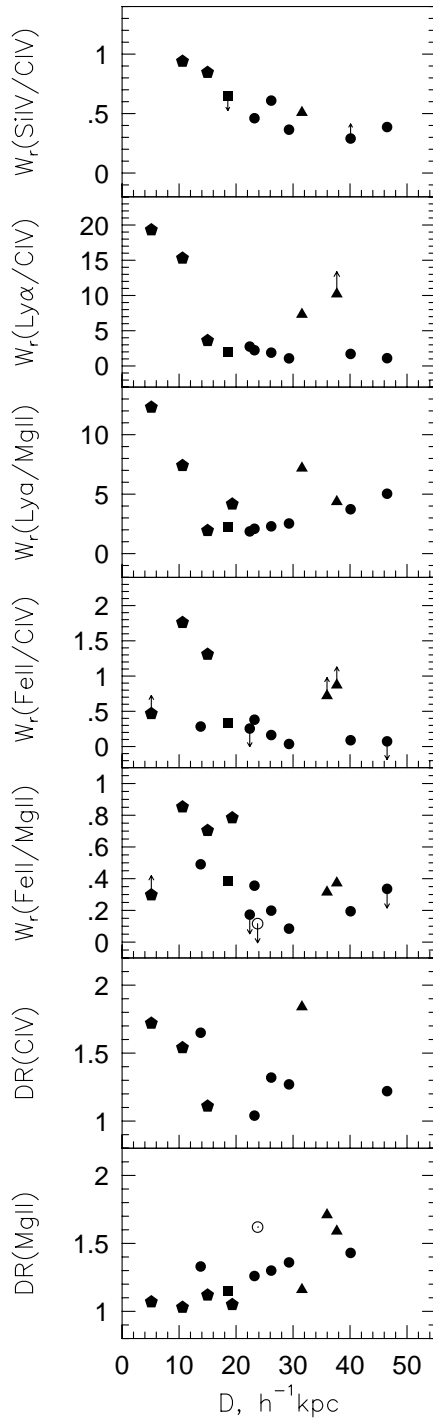
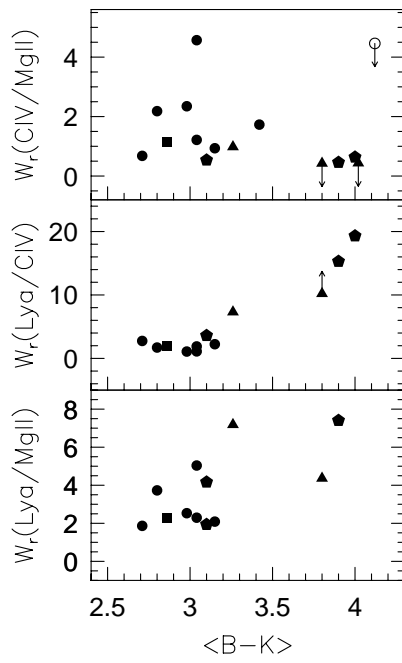


FIG. 11.— Selected equivalent width ratios vs. host galaxy impact parameters.

FIG. 12.— Selected equivalent width ratios vs. host galaxy $B - K$ colors.

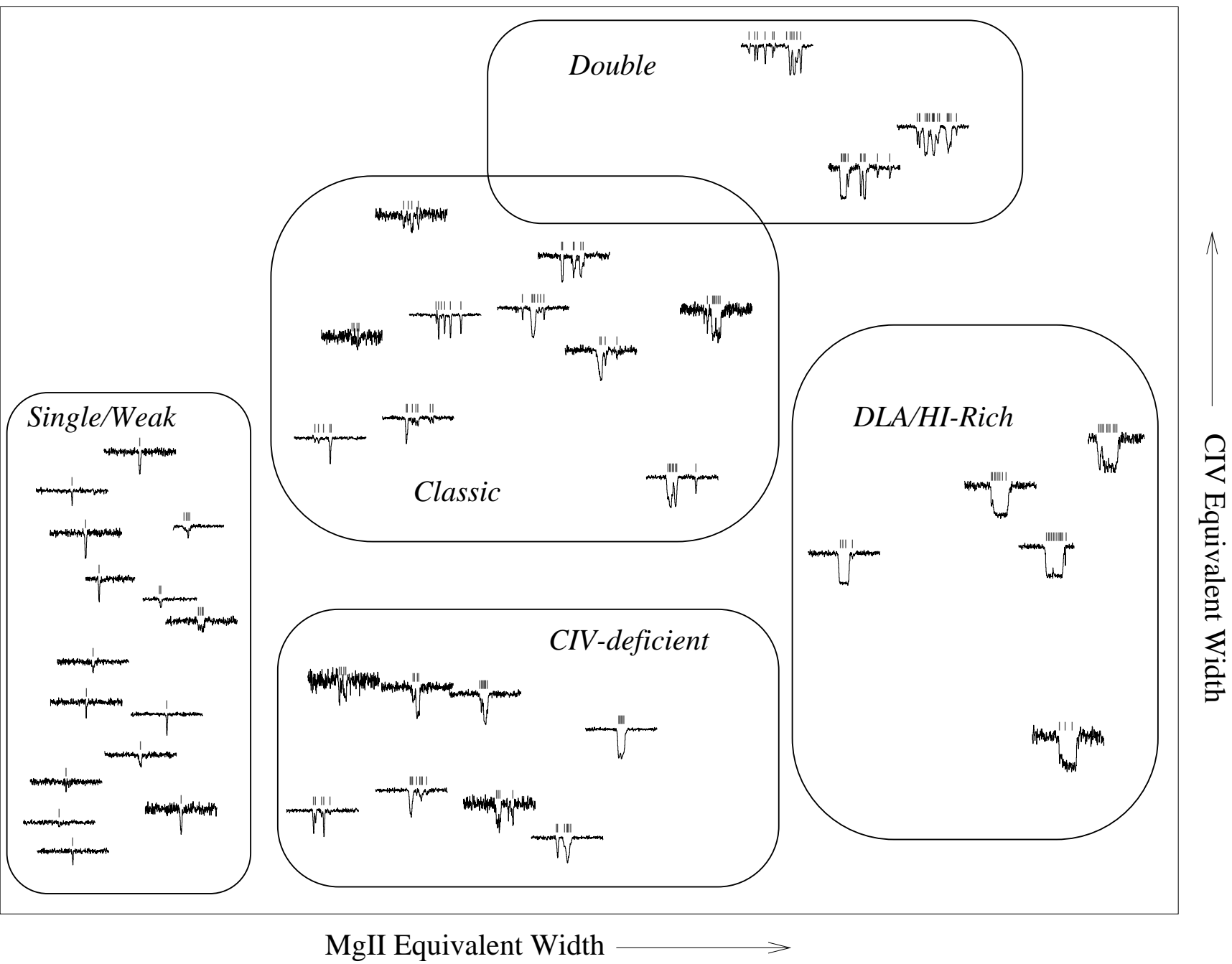


FIG. 13.— Taxonomy and the CIV–MgII kinematics connection. The MgII $\lambda 2796$ profile kinematics are placed roughly by their CIV and MgII strengths on the $W_r(\text{CIV})$ – $W_r(\text{MgII})$ plane. The loci of the taxonomic classes are schematically represented by the outlines.

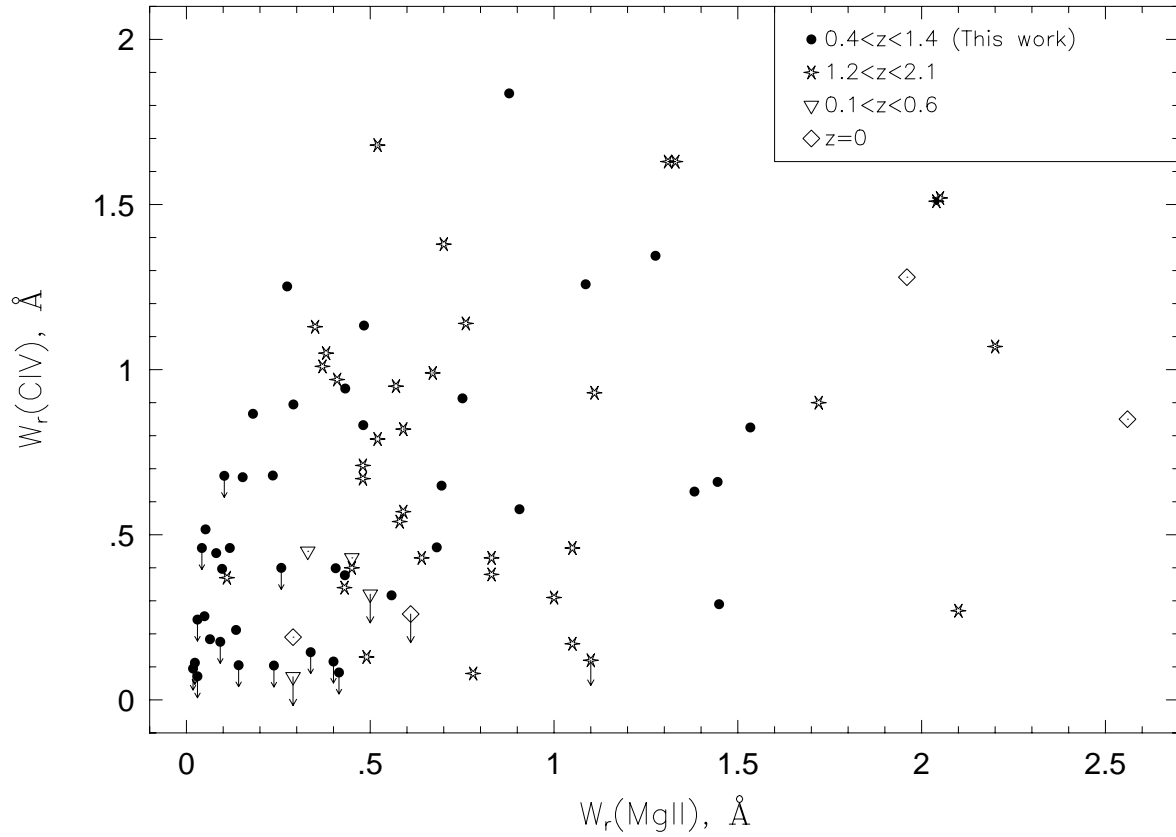


FIG. 14.— The $W_r(\text{CIV})$ – $W_r(\text{MgII})$ plane. Data from this study have point types the same as in Figure 3. Also plotted are: higher redshift points ($1.2 \leq z \leq 2.2$) from Bergeron & Boissé 1984, Boissé & Bergeron 1985, Lanzetta et al. (1987) Steidel & Sargent (1992) [six-pointed stars], lower redshift points ($0.1 \leq z \leq 0.6$) from Bergeron et al. (1994) [downward pointing, open triangles], and $z \simeq 0$ data from Bowen et al. (1996, 1996), and Bowen (private communication, 1999) [open diamonds].

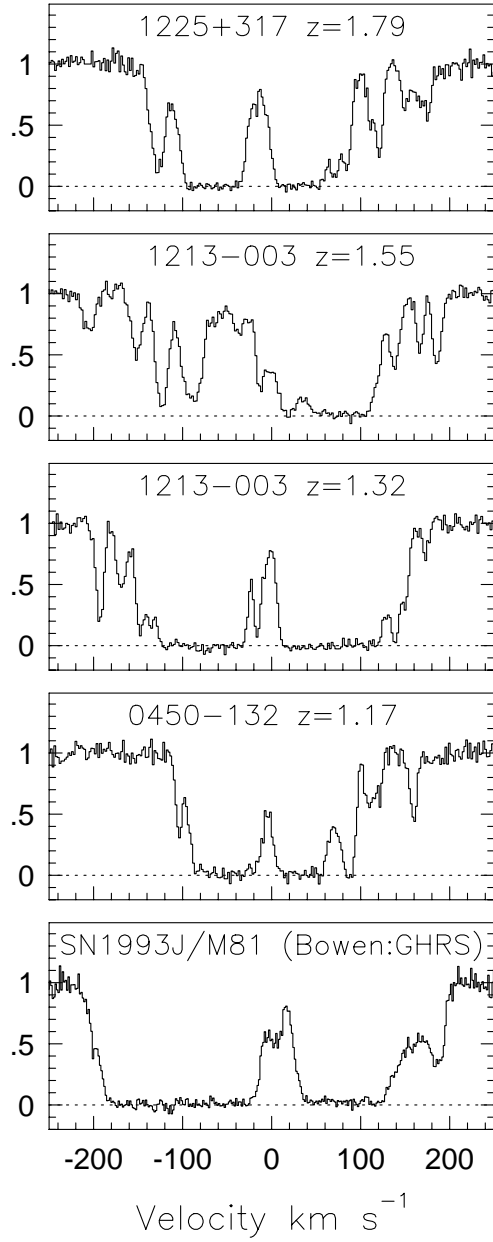


FIG. 15.— The Mg II $\lambda 2796$ profiles for four higher redshift systems and for the $z \simeq 0$ SN 1993J, a line of sight from the galaxy M81. These systems all have equivalent widths greater than 2 \AA . They occupy the extreme right portion of the C IV–Mg II plane (Figure 14) and are members of the population of the most rapidly evolving Mg II absorbers.